This is to certify that the

thesis entitled

PREDICTIVE TOOL WEAR OF COATED TOOL SYSTEMS

presented by

Raja Krishnan Kountanya

has been accepted towards fulfillment
of the requirements for

M.S. degree in Mechanics

Major professor

Date 4/22/98

PREDICTIVE TOOL WEAR OF COATED TOOL SYSTEMS

By
Raja Krishnan Kountanya

A THESIS

Submitted to Michigan State University

in partial fulfillment of the requirements

for the degree of

MASTER OF SCIENCE

Department of Materials Sciences and Mechanics

1998

ABSTRACT

PREDICTIVE TOOL WEAR OF COATED TOOL SYSTEMS

By

Raja K.Kountanya

Tool wear has been a serious concern in the economics of modern machining. In the light of the developments in materials technology, the demand for suitable cutting tool materials has entailed a detailed study into the various mechanisms that bring about tool wear.

Temperature has been known to play an important role in the mechanisms of wear of cutting tools. The literature is rich in studies that focus purely either on the temperature fields or the mechanisms that bring about tool wear. This study adopts a dual approach to the problem by empirical quantification of cutting temperatures and semi-analytical modeling of tool wear so as to eliminate the need for laborious testing for optimal tool materials. Abrasion [Rabinowicz, 1961] and chemical dissolution [Kramer and Suh, 1980] are understood to dominate the wear process of the tool for the work materials studied. Experimentally obtained wear data and that predicted theoretically, brought to light many interesting aspects in the tool wear problem.

Cutting tests were conducted on plain carbon steels of AISI designation 1018, 1045, 1065, 1070 and 1095 with carbide cutting tools with a single coating of TiN, TiCN and Al_2O_3. Temperature of the cutting tool was measured using an infrared pyrometer with a fiber optic attachment. An inverse estimation was then carried out to estimate the interface temperatures. Flank wear rate increased with cementite content. Crater wear rate increased with temperature attesting to the common notion that thermally activated wear mechanisms brings about crater wear. In general, good correlation between experiment and theory was found.

ACKNOWLEDGEMENTS

I wish to place on record my sincere thanks to my advisor Dr.Patrick Youngseon Kwon, for rendering all the technical and moral support during the course of this work. I am deeply indebted to his enduring patience and understanding, which was invaluable towards bringing this study to fruition.

My thanks to Thorsten Schiemann, from Aachen, Germany, whose insightful suggestions and practical knowledge clarified many a doubt, which arose during the experiments and the data processing. I consider my association with him as a delightful experience, which taught me the essence of teamwork. I am indebted to Ben Simkin, a fellow graduate student for his valuable time in obtaining the images on the Scanning electron microscope.

My thanks to my thesis committee members, Dr.Thomas Bieler and Dr.K.N.Subramaniam for their thoughtful suggestions in the writing of this thesis.

My thanks to Mr.Fritz Smydra of Lansing Community College for his expertise on the CNC lathe. His availability on some crucial weekends is deeply appreciated. My thanks also to Kurt Niemeyer and Mr.J.C.Brenton of the machine shop in the College of Engineering, M.S.U. for 'lending me a hand ' on many an occasion.

Last but not the least, my thanks to all my friends in and around campus, including Biman Ghosh, Sunil Chandran, Suhail Ansari, Monica Lokre and Sridhar Seshagiri whose encouragement was the 'magic tonic' to keep me going. The moral I gained from the whole experience was the simple truth in the sanskrit saying 'Siddhirbhavati Karmaja', meaning 'Do Unto Perfection'.

TABLE OF CONTENTS

LIST OF TABLES

LIST OF FIGURES

LIST OF SYMBOLS

KB	Crater width (μm)
KT	Crater depth (μm)
KM	Crater center distance (μm)
KA	Crater area (mm^2)
VB	Average wear land width (μm)
VB_{max}	Maximum wear land width (μm)
r	Nose radius of insert (mm)
V, V_m	Volume of worn material
θ	Roughness angle of the abrasive (deg)
x	Sliding distance (m)
L	Normal force of interaction between the surfaces (N)
P_t	Tool material hardness (Kg/mm^2)
P_a	Abrasive Hardness (Kg/mm^2)
A	Calibration constant for abrasive wear per sliding distance
B	Calibration constant for dissolution wear
C	Solubility (dimensionless)
M	Molar volume (cm^3/mol)
G	Gibbs' free energy (Kcal/mol)

G^{xs}	Excess free energy of solution (Kcal/mol)
R	Universal gas constant (kcal/mol.°K)
x,y,z	Stoichiometric coefficients
B_t	Volume worn away on the relief face (mm^3)
w	Flank wear land (mm)
α	Constant for the softening (/°C)
H	Hardness (Kg/mm^2)
T	Temperature (°C)
Θ	Dimensionless temperature
R_ξ	Distance in elliptical coordinates (mm^3)
a,b	Parameters describing the base ellipse (mm)
K	Complete elliptical integral of the first kind
T_r	Steady-State cutting interface temperature (°C)
T_∞	Temperature in the far-field of the tool (Taken to be 25°C)
MV	Molar Volume (cm^3/mol)

OVERVIEW

Metal cutting has been a field of study of immense commercial importance. Since even minor improvements in productivity can result in enormous cost savings and profits in high volume production, there has been a never-ending demand for research in this field even after ten decades of industrialization. In the light of the enormous amount of work done in the past and the work going on presently, the scope of research has become very focussed. Hence, study of any problem in metal removal processes involves careful design of experiments, instrumentation and evaluation of results. A solid infrastructure is therefore necessary for in this field.

Development of cutting tool materials has been foremost in all the research in related to metal cutting. A significant stride in this regard has been the innovation of adopting certain coating technologies for depositing thin hard coatings on common tool substrates. This technique, developed in the early 1970s, dramatically improved tool life and productivity. Today more than 75% of turning operations and 40% of milling and drilling operations are performed on coated carbides. While hot-hardness and chemical inertness have been recognized to be the two important parameters for coating materials, the exact dependencies and the rationalization are yet to take a concrete shape.

Chapter 1

INTRODUCTION TO TOOL WEAR

Cutting edge wear is still one of the unsolved problems in metal cutting. No matter how superior the tool material is, it is common experience that tool life, defined as the time for which tool wear is within acceptable limits, is always finite. Consequently, the reasons for interest in tool wear are threefold: (1) Lower workpiece quality due to deterioration in finish and dimensional accuracy, or damage to expensive workpieces if an edge fails catastrophically in a cut. The second is (2) the cost of changing cutting edges, the cost associated with the concomitant time delays and damage caused by unexpected failure and (3) the increased power consumption due to the excessive rubbing of the tool with the work material. Work continues for three basic purposes: (1) how to accurately predict wear, (2) how to detect wear from measurements while machining, and (3) how to minimize wear by the development of new materials. This study was focussed on the first purpose.

1.1 Geometrical Aspects of Tool Wear

In order to characterize tool wear the proper geometric parameters have to be defined. The ISO standard 3685-1977(E) [1] for tool life testing was formulated with this express purpose so that there can be a basis for comparison between various cutting tool materials. Figure 1.1 illustrates the geometric parameters associated with tool wear in a typical right hand turning tool.

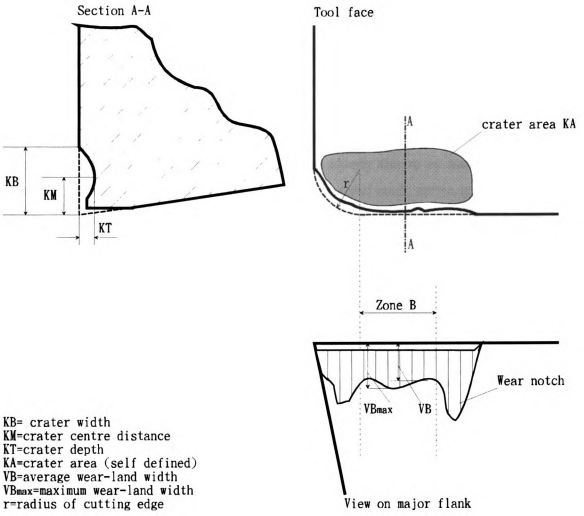

Figure 1.1: Zones of damage of the cutting tool due to machining

1.2 Literature Survey in relation to tool wear

In the light of the numerous attempts to investigate tool wear, the following section will detail briefly the important information gathered from the recent literature concerning this study.

Ramalingam and Wright [2] performed studies on well-characterized work materials such as Fe-C-silica powder-metallurgy compacts where they found flank wear to increase with silica content. They concluded that alloy chemistry did not describe machinability and found the wear process on the tool flank to be dependent on interfacial temperatures. The prowing action of the abrasive particles was clearly shown by means of quick-stop sections. They also concluded that while the tool material could soften considerably at the temperature prevalent at the interfaces, the abrasive particles did not soften by the same amount since the duration for which they were present in the shear zone was extremely small, of the order of milliseconds. Tool chip temperatures were higher for carbide tools due to the higher speeds used on them. A modest assumption that the flank temperature was 300-400°C lower than the chip-tool interface temperature was made.

Byrd and Ferguson [3] studied the influence of hard inclusions on flank wear of carbide tools. Al_2O_3 particles were artificially impregnated in 1020 and 4620 steels using the P/M technique. They concluded that higher temperatures encountered in the machining of steels do not in any way impede the abrasive action of hard inclusions in the microstructure. However, they also had difficulties in establishing a threshold level in the degradation of machinability due to hard particles in the microstructure. Vol.% of hard particles seemed to provide a clue to the machinability.

Brun *et al.* [4] performed experiments on 40%vol. SiC aluminum alloy with different tool materials. Since they were cutting aluminum, cutting temperatures encountered were expected to be low. They found that tool materials harder than SiC performed much better than the others. This dependence on hardness represented a complex behavior wherein abrasion was dependent on temperature at the interfaces and the altered

properties of the cutting tool at this temperature. Kramer [5] investigated the wear resistance of binary carbide coatings. The WC substrates began deforming thermally nearly at 1030K and showed a rapid decline in the compressive strength. At higher cutting temperatures, he concluded that chemical dissolution was the most important wear mechanism.

Ramalingam and Watson [6] considered the factors responsible for the scatter in tool life. The role and significance of the oxygen rich non-metallics on tool wear and machinability was examined. Tool chip interface temperatures of carbide tools were 800°C and above under normal industrial practices. Diffusion was excluded as a contributing wear mechanism since it was thought that diffusion was a well behaved, non-equilibrium mechanism that would lead to a deterministic solution for tool life. In carbide tooling the 'prowing' process was believed to give rise to plastic flow in the carbide at the tool-chip interface. Hence, a plausible reason for the stochasticity was the variation in distribution of the abrasive particles in the work material.

Kramer and Kwon [7] concluded that tool wear was primarily due to two mechanisms namely chemical dissolution and abrasion. The dissolution of the tool material in the moving stream of chip material may be treated as a dilute solid solution formation and can be modeled as a regular solution. They also concluded that even though wear models such as the 3-body and 2-body abrasion do not describe the constraints on the abrasive particle in machining, they can be adopted for modeling abrasive wear. The ferrite matrix was believed to be quite soft at the temperatures present in the zone of deformation during cutting, offering minimal restraint to the inclusions. The details of two-body and three-body abrasion, an important highlight of this study, will be presented later on in this thesis.

Kramer and Suh [8] developed the dissolution wear model, which will be the topic of discussion later on. They concluded that solution wear is predominant in the carbide class of tool materials, which is independent of the diffusion characteristics. In all cases the

tool material was assumed to be dissolving in α-iron. The solubility in γ-iron was excluded due to the commonly observed sluggishness of the α→γ transition. Essentially, this study proved that the free energy of formation of the ceramic coating determined the effectiveness of the coating. The hypothesis was confirmed from the ranking obtained from the experimental results of crater wear and that obtained from the thermodynamic calculations. The difference of this model from the formerly believed diffusion theory is that dissolution is an equilibrium process whereas diffusion is not.

Dearnley [9] cut various plain carbon steels carbide tools with a single or composite layers of TiC, TiN and Al_2O_3. Cutting temperature was measured using the tool-work thermocouple method and was further verified using the metallurgical technique. Uncoated tools showed a larger HAZ (Heat Affected Zone). The temperature difference between the uncoated tools and the coated tools was found to be less than 150°C. Although clear evidence of seizure was noted on the rake surface, there were indications of reduced interfacial contact on the flank. The Al_2O_3 coatings and the ceramic inserts showed the greatest propensity for ridges on the rake face via discrete plastic deformation giving further evidence to abrasion on the flank since temperatures are lower on the flank. This was the basis for the conclusion that wear of Al_2O_3 was primarily due to a decohesion mechanism. Moreover, flank wear trends never followed the trend indicated by the dissolution or diffusion mechanisms indicating that they may not be the rate controlling mechanisms, i.e. the mechanisms contributing the most to tool material removal, on the flank. However, they were useful in interpreting the preferential dissolution of the WC substrate.

Cho and Komvopoulos [10] studied wear mechanisms of multi-layered coated tools. Severe abrasion was noted at the flank because of the lower temperature than the crater, the more rigid work material and the constraint of the moving work and the tool. In the case of Al_2O_3, they noted that dissolution may be neglected at all cutting speeds and mechanisms such as plastic flow, thermo-mechanical fatigue and fracture were expected to prevail at all temperatures.

Cook [11] observed that the average wear land temperature seemed to approach the tool-chip interface temperature as tool wear progresses. At higher speeds, crater wear rates were primarily a function of the temperature. Functionality of flank wear with temperature was not deducible precisely. Stjernberg and Thelin [12] noted that increasing the coating thickness increased the overall resistance to crater wear. The time needed to expose the substrate underneath was the determining factor in this regard. It was suggested that the temperatures in the flank are 300°C lower than that at the chip-tool interface. All coatings were harder and more ductile at lower temperatures. Notch wear was noted to be a chemical phenomenon.

Kramer [13] suggested that at moderate cutting temperatures, excessive rubbing occurs between the flank and the work material. Flank wear determined tool life at low speeds due to mechanically activated wear caused by microfracture, thermal and mechanical fatigue and abrasion by hard inclusions. Milovic *et al.* [14] noted that the fluctuating stress conditions that can exist within the BUE in the machining of free cutting steels can be the reason for the superior performance of HSS tools as against carbide tools, owing to their superior toughness. The coating reduced the interface temperature by as much as 125°C and hence could be used to turn the material at a speed higher by 25 m/min. The thermal conductivity of carbide tools, which is higher than that for HSS, was another reason for the higher heat abstraction from the interfaces and hence higher speeds needed for machining without a BUE.

Chubb and Billingham [15] studied the wear mechanisms in high speed machining. They found that once the coating was removed from the flank, the mechanism of wear appeared to be a combination of abrasion and diffusion. WC appeared to wear by diffusion as evidenced by the smooth boundary between the WC particles and the steel. Hence tool life due to flank wear was closely related to the breakdown of the coating on the flank. Kim [16] noted that abrasive wear dominated the wear on the flank surface and diffusion on the crater surface. He also concluded that excessive coating thickness could retard wear performance.

Kim and Durham [17] noted that cutting temperature as high as 1600°C could be reached with alumina tools without tool failure. The temperature at the flank could be 100°C lower. Tools with a higher thermal conductivity and a higher hot hardness showed a higher resistance to flank wear. Lee and Richman [18] noted that coated tools resist cratering even after the coating had been removed in some places. Hardness of a material as a coating was noted to be very different from that as a bulk material. Cooling of CVD coatings after deposition at 1000°C was noted to develop tensile residual stresses in them. Hardness measurements on coatings were particularly difficult because of the smooth surfaces that are demanded for accurate measurements.

Suh [19], in his classic paper, outlined the essential ingredients for the making of high performance coatings. Both mechanically and chemically activated wear processes were pronounced to depend sensitively on temperature. In general, though tools should be at least 4-4 1/2 times harder than the work material, this is not applicable to coatings since crater wear rates and hardness of the coatings did not correlate very well. Residual stresses existed in the coatings and were a function of the CTE differences between the coating and the substrate. An important point made in connection with this study is that contrary to Al_2O_3, SiC or SiO_2, Fe_3C has a very high free energy of formation and is likely to dissociate at high temperatures. There has however, been no experimental evidence to date in this regard. He also mentions that Al_2O_3 coatings may have problems adhering to the substrate since Al_2O_3 did not permit diffusion of carbon atoms across the interface which relates to the common experience of depositing an intermediate layer of an adherent material like TiN, as was the case in this study.

Subramaniam *et al.* [20] performed high speed machining on AISI 1045 steel. They noted that crater area increased with cutting speed. Evidence of twinned martensite in the chips quenched in water were in accord with the average interface temperature predictions for the secondary shear zone since steel undergoes a martensitic transformation at these temperatures. The thermodynamic potential for dissolution is the

most important criterion for the design of a coating to minimize crater wear at high speeds.

Trent [21,22,23] is one of the pioneers in recognizing the exact interfacial conditions on the rake face. He was also the first to perceive the importance of recognizing the mechanisms that control tool wear. In his 1963 series of papers, he was the first to depart from the then accepted notion of the interfacial conditions. It was then believed that there was relative motion between the chip and the tool on the rake face. It has now been established beyond doubt that chip flow resembles fluid flow with an initial region where there is relative movement and thereafter there is complete seizure thereby forming the 'secondary' shear zone. Among the other pioneers in the field are G.Boothroyd, P.L.B.Oxley, O.Optiz and M.C.Shaw. Their innumerable contributions to the literature have enabled a very scientific understanding of metal cutting today.

1.3 Importance of Temperature in relation to tool wear

From the above section the importance of cutting tool temperatures in tool wear can be appreciated. Not only does a higher temperature bring about softening of the tool but it also makes the cutting tool vulnerable to thermally-activated mechanisms such as dissolution and diffusion. It can also be seen from the literature survey that only a few attempts have been made at a thorough quantitative study of tool wear involving temperatures. The present study will create precedence for one in the future so as to enable a very scientific and rational framework for predictive tool wear.

Chapter 2

STATEMENT OF THE PROBLEM

The principal aim of this study is, as mentioned before, is a quantitative study of tool wear involving cutting tool temperatures. Among the various mechanisms, which have been presented in the literature, two main mechanisms namely, abrasion and chemical dissolution are selected and formulated for the purpose. A calibration scheme is then proposed wherein tool wear can be predicted for a given cutting temperature.

2.1 Rabinowicz Three-Body and Two-body Abrasive Wear Models

Among the various abrasive wear models in tribology literature, the one appropriate to modeling abrasive tool wear is the three-body abrasive wear model. Rabinowicz *et al.* [24] performed experiments wherein two surfaces slid against each other with the abrasives introduced in-between [Fig.2.1]. They drew conclusions related to wear rates, sliding conditions and material hardness. A number of materials and abrasives were chosen and a general empirical relation was found to fit the data. The final form of the equations, as applicable to tool wear, is as shown in equations 2.1.

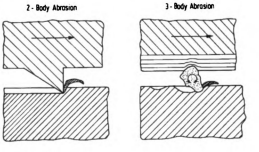

Figure 2.1: Illustration of two-body and three-body abrasion.

$$V_m = \frac{xL\tan\theta}{3P_t}, \qquad \frac{P_t}{P_a} < 0.8$$

$$V_m = \frac{xL\tan\theta}{5.3Pt}\left(\frac{P_t}{P_a}\right)^{-2.5}, \qquad 1.25 > \frac{P_t}{P_a} > 0.8 \qquad \textbf{Equations. 2.1}$$

$$V_m = \frac{xL\tan\theta}{2.43Pt}\left(\frac{P_t}{P_a}\right)^{-6}, \qquad \frac{P_t}{P_a} > 1.25$$

where $\tan\theta$ is the average tangent of roughness angle of the abrasive grains (a measure of the particle shape or sharpness), x is a sliding distance, L is the normal force of interaction between the surfaces, P_t is the hardness of tool and P_a is the hardness of the abrasive. Eqs. 2.1 calculate the abrasive wear volume as a function of a sliding distance, x.

In theory, the equations always governed the volume of material removed, unless the process of abrasion was preceded by the formation of cracks. In the presence of cracks, material is removed by brittle fracture as well as by abrasive wear. Since the tool wear pattern usually seen on the flank, which consists of characteristic groove marks, resembles a plastic ploughing process, the empirical relations can be expected to describe three-body abrasion in tool wear also.

While three-body conditions exist when two bodies slide against each other with the simultaneous rolling of a hard abrasive particle in-between, two-body conditions represent a hard surface sliding over a relatively soft surface. The relations for two-body wear are relatively simpler. The volume removed per sliding distance is expressed in equation 2.2.

$$\frac{dV}{dl} = \frac{L\overline{\tan\theta}}{\pi p_t} \qquad \textbf{Equation 2.2}$$

where L = Load between interacting surfaces

θ = angle for indentation of the conical abrasive particles

p_t = hardness of the abraded surface, here the tool flank.

It should be noted that, in this model, the hardness of the abrasive does not appear in the relation for the wear per sliding distance. Also the hardness of the abrasive is assumed to be infinite. Figure 2.2 shows the schematic used to obtain the relation.

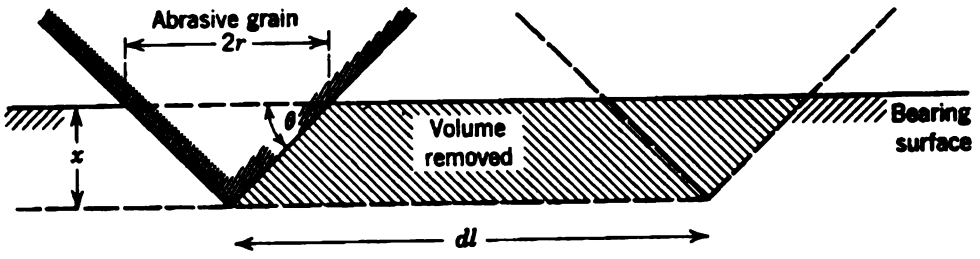

Figure 2.2 Oversimplified model of a conical abrasive wearing a bearing surface to illustrate abrasive action

2.2 Chemical Dissolution Wear of Kramer and Suh

Kramer and Suh [8] treated crater wear as an equilibrium process of dissolution and that a thermodynamic potential existed for the solution of the tool material in the chip material. They obtained excellent correlation between the wear rates predicted by theory and that from experiment. This is in opposition to the thermal process of diffusion, which was then widely believed to be the cause of crater wear, since diffusion is a non-equilibrium rate process. Diffusion kinetics [8] were proved to be relatively slow at normal cutting temperatures. Figure 2.3 shows the schematic used to describe the phenomenon.

The solution wear rate, in terms of the solubility and other parameters, is given by equation 2.3.

Chemical Dissolution Wear Rate = $\left[BMCV^{0.5}\right]$ **Equation 2.3**

where M is the molar volume, C is chemical solubility of the tool material in the work material, V is the cutting velocity and B is a calibration constant. The 0.5 power in the velocity term comes from the Schmidt number in mass transfer [7].

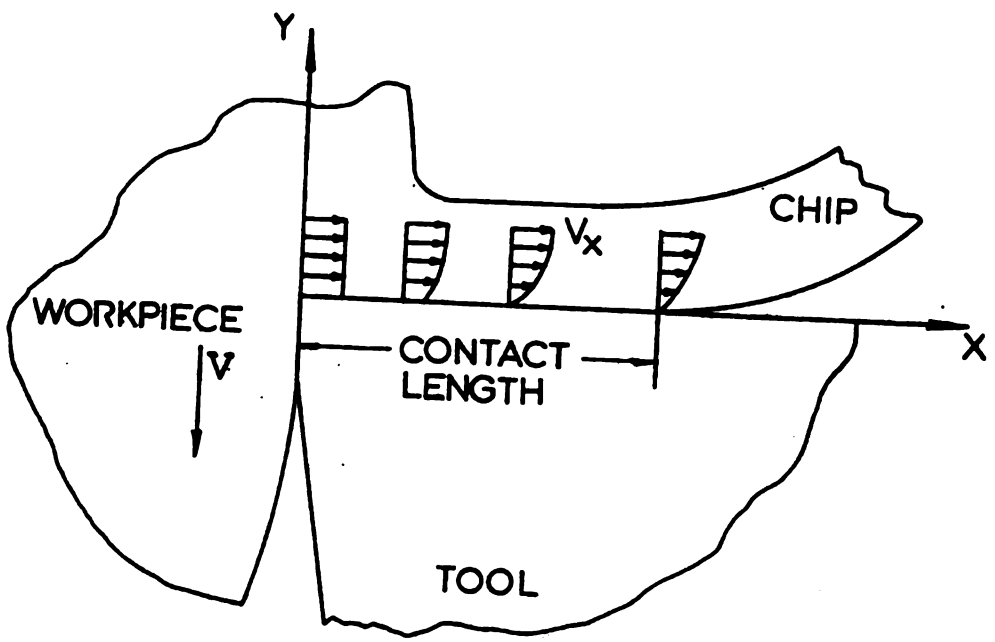

Figure 2.3: Schematic illustrating chip flow and continuity conditions [Kramer and Suh, 1980]

For a compound $A_xB_yC_z$, the solubility is given by equation 2.4.

$$C_{A_xB_y} = Exp\left[\left(\frac{\Delta G_{A_xB_y} - x\Delta\overline{G^{xs}}_A - y\Delta\overline{G^{xs}}_B - z\Delta\overline{G^{xs}}_C - RT(x\ln x + y\ln y + z\ln z)}{(x+y+z)RT}\right)\right] \quad \textbf{Equation 2.4}$$

where

$\Delta G_{A_xB_yC_z}$	=	Free energy of formation of the tool material
$\Delta\overline{G^{xs}}_A$	=	Excess free energy of solution of component A in the chip
$\Delta\overline{G^{xs}}_B$	=	Excess free energy of solution of component B in the chip

$\Delta\overline{G^{xs}}_C$	=	Excess free energy of solution of component C in the chip
R	=	Universal gas constant
T	=	Absolute temperature in Kelvin

Notes

1. α-Iron is assumed to be the phase into which the tool material dissolves even though the transformation to the γ-phase occurs at 996K.
2. Regular solution behavior is assumed.

Because **A** and **B** cannot be determined directly without experiments, the previously discussed models can predict only relative wear rates where relative wear rate is defined as a ratio of wear rates between a candidate coating material and a reference coating material.

2.3 Comprehensive Models for Crater and Flank Wear

Many workers [10,15] have enunciated flank wear to be a case of pure abrasion. Hence flank wear can be modeled as a case of abrasion alone [equations 2.1, 2.2] and hence wear needs to be calculated as a wear volume for this purpose. Furthermore, It is widely believed [11,16] that flank wear rate is best expressed on a sliding distance basis in view of the fact that unequal cutting times can give a distorted picture of flank wear.

It can be seen in Shaw [25] that

$$B_t = \frac{bw^2 \tan\theta}{2} \qquad \textbf{Equation 2.5}$$

Where B_t	=	Volume worn away on the relief face
w	=	Wear land on the tool
θ	=	Relief angle of the tool.

Hence the wear volume on the flank is proportional to the square of the wear land. Since the Rabinowicz model calculates wear on a sliding distance basis, the appropriate

[25] formula for calculating the abrasive wear rate on the flank derived from equations 2.1 and 2.2 is shown in equation 2.6.

Flank volume wear per Sliding Distance $= AK\,(P_a^{(n-1)})/(P_t^n)$ (3-body abrasion)

$= A(1/Pt)$ (2-body abrasion)

Equations 2.6

where K is the factor from Equations 2.1. Experimentally obtained wear land values have to be expressed as $(VB)^2$/Sliding-Distance[1] [Figure 1.1] to correspond to the abrasive wear calculation and *A* is a constant to be obtained from experiments.

For modeling crater wear, one has to account for both mechanisms [13]. Wear rate has to be expressed on a time basis since the dissolution wear rate is not expressible on a sliding distance basis. Therefore [7,8]

Crater Wear Rate $= [AVK\,(P_a^{(n-1)})/(P_t^n) + BMV^{0.5}\,C_{AxByCz}]$. **Equation 2.7**

It is therein assumed that the abrasive and dissolution volume wear rates are directly proportional to the crater depth and hence experimental wear rate is simply KT/cutting time [Figure 1.1].

2.4 Accounting the variation of hardness with temperature

Most importantly, one has to consider the thermal softening of the tool and the abrasive while machining. A suitable relation has to be evolved to account for the softening of the materials concerned. Kramer and Kwon [7] used an exponential function of the form of equation 2.8,

$$H(T) = H_0 e^{-aT} \qquad \textbf{Equation 2.8}$$

[1] Sliding-distance (m) in a turning operation is cutting velocity (m/min) × cutting time (mins)

where $H(T)$ was the hardness of a material at a given temperature T°C. H_0 and α are constants obtained form a curve fitting process on the empirical data. In the present analysis, the same form is adopted along and developed along with the other thermophysical properties in the computer algorithm to be described later on.

2.5 Comparison with Taylor's model for tool wear

F.W.Taylor was perhaps the first person to recognize the importance of cutting tool materials to modern civilization. Often proclaimed as the co-inventor of high-speed steel, his tool life criterion has been in use ever since he came up with it. Stated simply as in equation 2.9, it relates various process parameters and the tool life in an heavily empirical form.

$$VT^n a^m f^l = C \qquad \textbf{Equation 2.9}$$

where V is the cutting velocity, T is the tool life, a is the depth of cut, f is the feed and l, m, n and C are constants obtained from a series of machining tests performed as specified in the ISO standard 3685-1977(E) [1].

However, simple as it may be, from the standpoint of adoption in the industry, it cannot be sustained indefinitely since a large number of work materials such as metal matrix composites and multi-layered coated tool materials, with a equally enormous number of geometries, are now becoming available. Not only does tool life has to be known apriori for given process parameters, the predictability of the machining process is equally important because of the close tolerances and stipulations being made nowadays on the surface finish of the component.

Chapter 3

CUTTING TOOL TEMPERATURES

Temperatures in metal removal processes have long been of interest to many researchers. There are essentially three temperatures to be concerned with in the turning process [Figure 3.1], (1) the shear plane temperature, which represents the bulk of heat generation in the chip formation process, (2) the chip-tool interface temperature, which is influenced by a number of factors including the secondary shear zone and (3) the flank temperature or the work-tool interface temperature, which is considerably lower than the other two. Flank temperature is important for its influence on the wear mechanisms prevalent at the flank in addition to its minor contribution to the heat generated in the chip-formation process. This chapter elaborates on the theory for the temperature measurement in the experiments conducted.

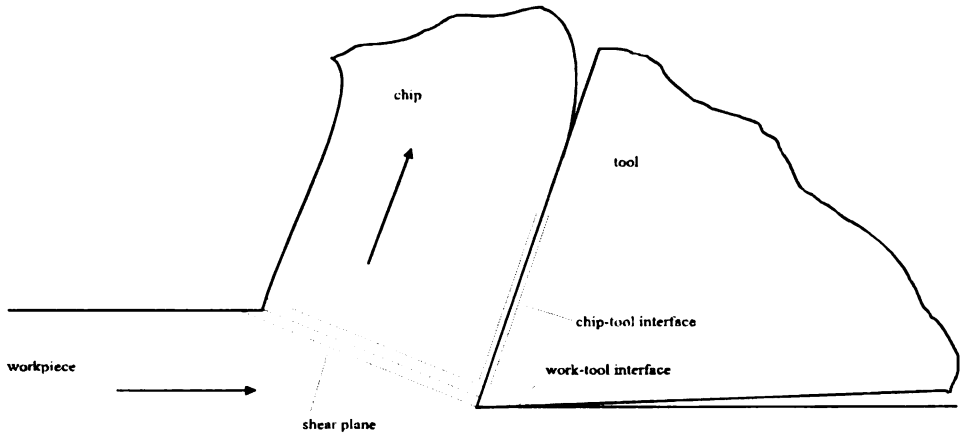

Figure 3.1: Sources of heat generation in a cutting tool

3.1 Inverse Problem of measuring interface temperatures

Cutting tool temperatures are usually measured using a chip-tool thermocouple technique [11]. This technique essentially gives the area weighted mean of the temperatures at the chip-tool interface, the work-tool interface and the shear plane. Other models developed recently such as the 1D ellipsoidal model of Yen and Wright [26] avoid the problem of inaccessibility of the interfaces and determine the cutting tool temperature as a whole field measurement and thus enable inverse estimation of interface temperatures. These involve measuring the cutting tool temperature away from the interface and adopting an inverse estimation of the chip-tool interface temperature.

3.2 1D ellipsoidal model of Yen and Wright[26]

The model essentially assumes that a one-eighth ellipsoid [Figure 3.2] in the domain of the cutting tool represents an isothermal surface. The cutting tool is therein assumed to be a semi-infinite body. Heat generated at the shear plane and the chip-tool interface manifest themselves as heat input into the cutting tool in a defined elliptical area of contact on the rake face. This heat input is represented as a constant temperature in this elliptical area and used as the boundary condition for the heat diffusion equation.

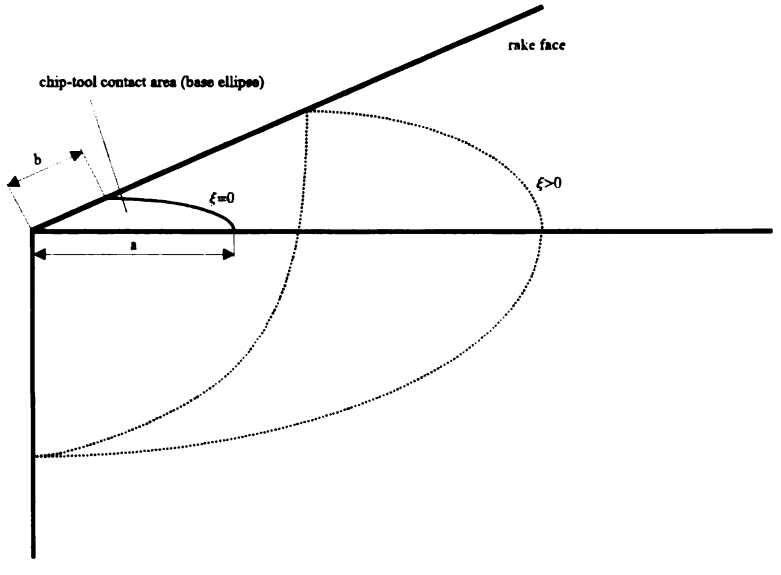

Figure 3.2: Temperature distribution in a cutting tool for the inverse temperature estimation

For the steady state temperature distribution, one has to solve the Laplace equation in ellipsoidal coordinates. However, it can be simplified for the special case of the one-dimensional (1-D) steady-state problem, where the temperature distribution in the tool body is a function Θ, only of the radial coordinate ξ as in equation 3.1[26].

$$\frac{d}{d\xi}\left(R_\xi \frac{d\Theta}{d\xi}\right) = 0 \qquad \textbf{Equation 3.1}$$

with $R_\xi = \sqrt{(a^2+\xi)\cdot(b^2+\xi)\cdot\xi}$ and $\Theta = \dfrac{T_\xi - T_\infty}{T_R - T_\infty}$

where ξ is the radial coordinate in the 1-D ellipsoidal model [mm^2]

a,b are the parameters describing the base ellipse with a>b [mm]

Θ is the relative steady state temperature

T_R is the steady-state chip-tool interface temperature [°C]

T_ξ is the temperature at the location determined by ξ [°C], and

T_∞ is the ambient temperature [°C].

The boundary conditions specified are: -

1. All other faces are insulated (heat convection = 0 or negligible).
2. Thermophysical properties of the tool material are constant.
3. The tool is rigid and tool wear is negligible.
4. Uniform temperature T_R at the chip-tool interface.
5. Temperature at infinity or the far field of the tool is T_∞.

With some mathematical manipulation, a function for Θ can be found as in equation 3.2.

$$\Theta(\xi) = 1 - \frac{a}{2K(m)}\cdot\int_0^\xi \frac{1}{\sqrt{(a^2+x)\cdot(b^2+x)\cdot x}}dx$$

$$= 1 + \frac{iF\left(Sin^{-1}\left(\sqrt{-\frac{\xi}{b^2}}\right)\middle|\frac{b^2}{a^2}\right)}{K\left(\frac{a^2-b^2}{a^2}\right)} \qquad \textbf{Equation 3.2}$$

with $m = \dfrac{a^2 - b^2}{a^2}$

where $F(\xi \mid \alpha)$ is the complete elliptical integral of order α.

$K(m)$ is the complete elliptic integral of the first kind, and

x is a variable of integration.

The final form of the solution for the one-parameter case ($a = b$) appears as: -

$$\frac{T - T_\infty}{T_r - T_\infty} = 1 - \left(\frac{2}{\pi}\right) \tan^{-1}\left(\sqrt{\left(\frac{x}{a}\right)^2 - 1}\right) \qquad \textbf{Equation 3.3}$$

where

T_r is the steady-state cutting interface temperature

T is the steady-state remotely measured rake face temperature

T_∞ is the temperature in the far field of the tool (Taken to be 25°C)

x is the distance of the point of measurement from the origin of the axes, and

a is the radius of the circular tool-chip contact area.

While the model can be developed more generally for three dimensions, closed form solutions exist only for the 1D case with one, two or three parameters. The one-parameter scheme is extremely efficient and facilitates accurate computation of the interface temperature. Hence from knowledge of the temperature at a point located remote to the interface, i.e. at a distance x from the interface, the mean interface temperature at the interface can be estimated using equation 3.3. This is the form for the inverse estimation which was used in this study.

The inverse estimation scheme is however sensitive to measurement error, Lin *et al.* [27], while implementing it for the infrared method, concluded that the inverse predictions for the heat conduction problem is an ill-posed problem and instabilities are

likely. However, they established that temperature measured in the IR system was in agreement with that predicted by the metallurgical approach at low cutting speeds without chip control. They had also used a square tool in their experiments. Hence small deviations from theory are likely in using the same scheme for tools with a clearance angle, as in this study. The cutting speeds for which the effectiveness of the scheme was tested was also comparatively higher than that used in this study.

In a similar approach, Rall and Geidt [28] concluded that most of the energy in the the metal cutting process appears as heat that is transferred to the chip, even though the small proportion of heat transferred to the tool influenced tool life.

3.3 Oxley's method of obtaining the flank temperature

The temperature difference between the chip-tool interface and the flank has been a much debated topic. In the literature survey presented before, one can see a number of opinions raised regarding this. In this study, the relation proposed by Oxley [29] was undertaken. Oxley's conclusions were drawn from the isotherms of the infrared photographs taken by Boothroyd in an earlier work [30] where stresses and temperatures on the flank wear land were studied. Boothroyd's work also concluded that large variations with temperature do not occur (<16°C) over the flank wear land and that temperature was higher away from the cutting edge.

Stated simply, the tool work interface temperature is 0.82-0.95 times the mean chip-tool interface temperature (All temperatures being in Kelvin). An average value of 0.89 was used for this study. Slight deviations are possible due to the sharp HSS tools used in the Boothroyd's tests [30]. Moreover, the higher thermal conductivity of the carbide tools [12] would tend to make this factor higher than that for HSS. In the absence of an exact dependency, this nevertheless suffices for this context.

Chapter 4

EXPERIMENTAL WORK

4.1 Turning Experiments

The experimental work was carried out at the premises of the Lansing Community College in Lansing, MI. The machine used was a Milltronics Manufacturing 20 HP medium sized lathe with provisions for infinitely variable speed and programmable feed and depth. It had a rigid tailstock, important for ensuring minimal chatter while turning long bars. The lathe was facile since the RPM could be controlled to keep the cutting speed constant. Figure 4.1 shows the photograph of the lathe with the experimental set-up.

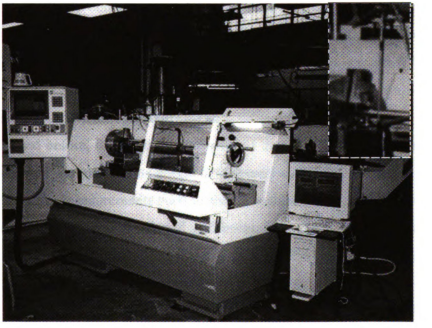

Figure 4.1: Photograph of the lathe with the experimental set-up (Inset: pyrometer end probe)

4.1.1 Cutting conditions and related issues

Dry cutting experiments were performed at a constant feed of 0.356 mm/rev (0.014"/rev) and depth of 1.905 mm (0.075") while the cutting speeds selected were at 300, 500, 700 and 900 sfpm (between 90 to 275 m/min). Cutting speeds were chosen after referring to the insert manufacturer's recommendations. The feed and depth of cut were determined after a few trial runs with the inserts to give a consistent cut with minimal chatter, sparking and good surface finish while maximizing on cutting time to reach steady state cutting conditions. The machine was also programmed for the RPM rather than the cutting speed to keep the cutting velocity constant.

A rigorous study of flank wear has to take into account this effect of the "cut-in" wear, which develops on the flank immediately after the commencement of cutting. Dearnley [9] had noted that flank wear rates estimated after longer cutting times were more representative than that after shorter cutting tests. In all cases at least a minute of cutting time was achieved to supercede the effect of this cut-in wear and ensuring that the tool reaches a steady state of wear. Exactly one cut was performed for every satisfactory data point. Data sheets consisting of the wear data and the process parameters were prepared for every cut and were compiled separately both as a hard copy and on the computer. The machining data (cutting speed) is shown in tables 4.6 and 4.7.

4.2 Method of Temperature Measurement

As explained before, there are several ways to measure cutting tool temperatures. In this study, infrared pyrometry was adopted. Conventionally this method is suitable only for high temperature measurements such as that in ovens and other places. However, new detector materials have been developed and hence this efficient and quick way of non-contact temperature measurement has become accepted all over the world. This method was deemed more reliable than other methods of cutting tool temperature measurement such as embedding thermocouples because: -

1. Bonding of thermocouples to the cutting tool is always a problem, given the dynamic nature of the process.

2. Thermocouples will tend to thermally 'load' the cutting tool and may alter the temperature patterns on the tool.
3. The pyrometer technique is reputed for the fast response it possesses.
4. Since the volume of cutting tests to be performed was very large, a non-contact method saves a lot of time in interchanging and indexing the cutting tool.

Coupling of fiber optics to infrared detectors represents the latest progress in the field of non-contact temperature measurement and control. Previously, fiber optics was excluded from consideration since they were made of glass and plastics, which are opaque to infrared radiation. This attachment can be beneficially used in cutting tool temperature measurement since it allows the probe to travel along with the cutting tool during the feed.

4.2.1 Principles of Infrared Pyrometry

The underlying principle of this technique is that all matter emits electromagnetic radiation at a temperature above 0K proportional to the fourth power of the absolute temperature. A temperature dependent emissivity is the parameter that adds a dimension to the physics of the method. Though emissivity itself carries several meanings according to the circumstances, it represents the behavior of a real surface and can be generally defined as the *ratio* of the radiation emitted by the surface to the radiation emitted by a black body at the same temperature.

4.2.2 Implementation of the Infrared Pyrometer for the experiments

The detector head of the pyrometer was designated OS1513 General Purpose Sensor used in conjunction with Model 3026 Single Channel Thermal Monitor[1]. It possessed a response time of 10-msec and was calibrated for the temperature range of 84-300°C. The end probe of the fiber optic cable was a glass tipped steel probe of 3" length (Not as shown in the photograph in figure 4.1) and the spot size was found to be 0.785 mm^2 prior to the commencement of every cut. Accurate positioning of the probe was

[1] Courtesy OMEGA Vanzetti, Inc.

done using a backlight source. There was also a provision for emissivity correction in the system, though this was not used in this study. The calibration of the pyrometer was performed using the BB-4 black body calibration source[1]. The non-linearity was found to be less than 1%. The absolute accuracy of the pyrometer was found to be 3°C.

Since the detector head was capable of measuring radiant energy in only one wavelength i.e. a single color pyrometer, it had to be corrected for the emissivity. Emissivity is always an important consideration in such non-contact temperature measurements especially while using these techniques for metallic surfaces, which are usually shiny. A high emissivity is desirable since it eliminates the adulterating effect of the background radiation. Among the coatings used for the testing, the TiN and TiCN inserts had a very shiny surface. In a concurrent study that was carried out, the emissivity of the TiN surface was found to be 0.101, which was dangerously low for temperature measurement.

To circumvent these problems, a thin coating was black high temperature paint (Flat Black) was sprayed on the inserts prior to the tests. Proper drying of the paint was ensured since this could harm the measurement during the experiments. The emissivity of this paint, which was known to be 0.92 from OMEGA, was the value to which the monitor always set. It is recommended that in future, the dual color detector head be used since this can measure temperature independent of emissivity.

1 Courtesy OMEGA Inc.

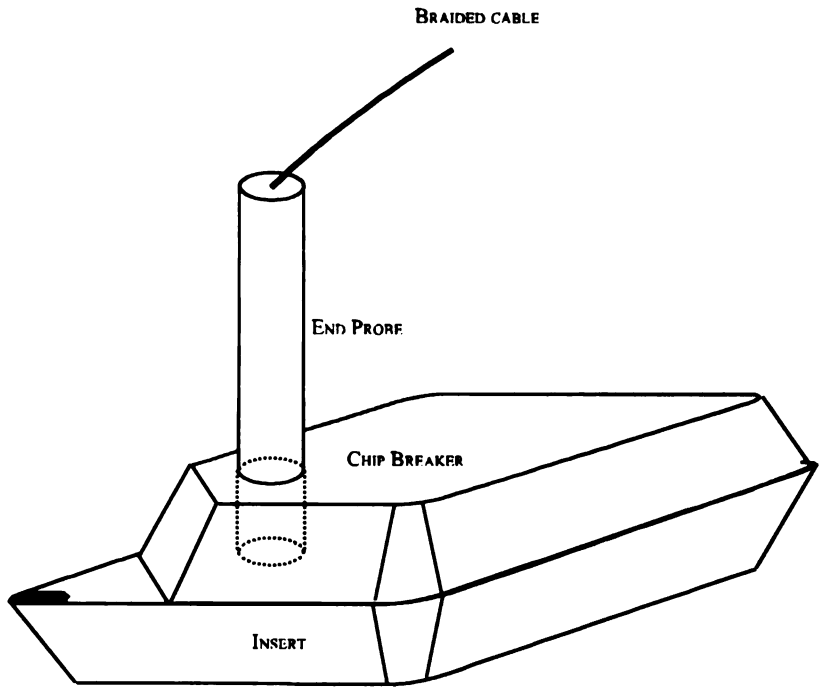

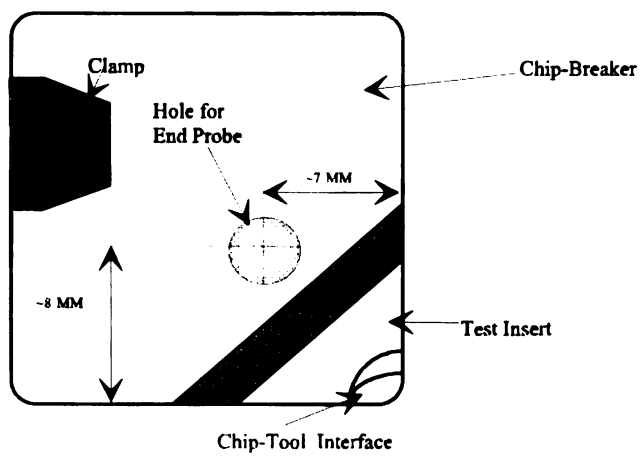

Figure 4.2: Illustration of the chip-breaker set-up over the insert

In order to prevent the interference of the chip in the field of view of the infrared probe and to exercise some control on the chip, a chip breaker was designed using one of the same inserts to hold the pyrometer in place. Figure 4.2 shows the schematic of the set-up shown to illustrate this point. It should be noted that there might be some disturbance in the temperature field due to this device. But in all cases it was found that it was sufficiently far away from the interface as shown in figure 4.2. The final assembly is as shown in figure 4.3.

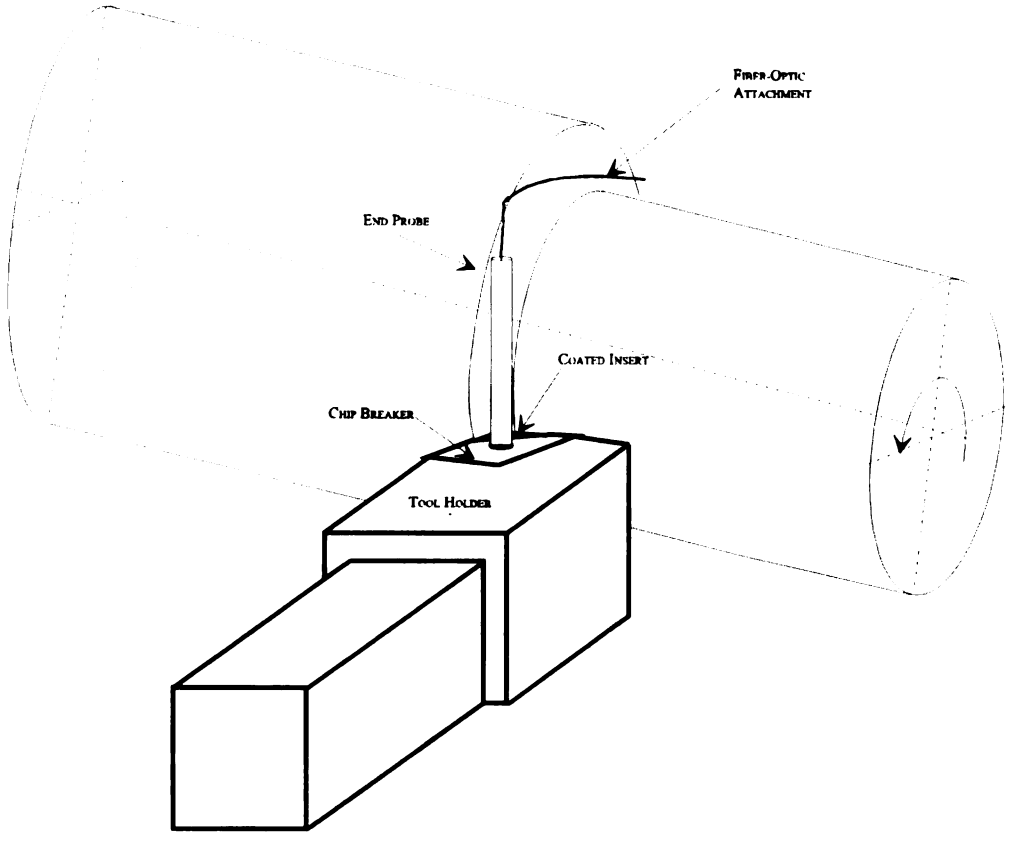

Figure 4.3: Final assembly of the pyrometer over the insert

4.3 Data Acquisition

Temperature data was collected in an automated data collection system. This consisted of a data acquisition board, signal conditioning and software which was written for the purpose of collecting and storing the data in a spreadsheet. The timer of the

computer was used, enabling the on-line monitoring of the temperature. Though initially the software was written for acquiring data in 5 channels-2 temperatures and 3 cutting forces, only the channel for the pyrometer was ultimately used. The thermocouple underneath the insert and the dynamometer were not implemented.

4.4 Work Materials

The work material consisted of steel rounds with the AISI designation 1018, 1045, 1065, 1070 and 1095. Being plain carbon steels, cementite constitutes the bulk of the inclusions in their microstructures. All the work materials for the experiments were procured from Alro Steel Corporation, Lansing, MI excepting the AISI 1065 bar, which was acquired from Timken as a compliment. It was learnt that the AISI 1065 steel was more commonly used as a plate rather than as a bar stock in the industry.

4.4.1 Dimensions of the bar-stock, cutting length and duration of cuts

The work material used for the experiments were steel rounds commercially obtained from ALRO Steel, Inc., Lansing, MI. The bar stocks were nominally of diameters between 3" and 6" and length was about 2-1/2' initially. The 1065 bar alone was 2" in diameter to begin with. However, all the bars had been reduced to a diameter of about 1.5" at the end of the tests. The cutting length was different for different bars for stability reasons. As mentioned before, the shortest cutting time was 1 min and 3 sec.

4.4.2 Spherodizing-annealing of the steels

The spherodize-annealing process transforms the cementite in the steel in to spheroids and brings the steel to a dead-soft condition, thereby removing any shape effect in the abrasion of the tool while machining. Those that were required to have a spherodized microstructure (1018, 1045, 1065 and 1095) were sent for heat treatment to Atmospheric Annealing, Inc., Lansing, MI. The sheer size of the bars excluded any possibility of annealing in a laboratory. This was also the reason due to which control over the grain size of the cementite in the steels was not possible. The as-received steels for the tests (1018, 1045 and 1070) were mainly in a hot-rolled, normalized condition.

The details of the annealing process for the AISI 1045 steel is shown below: -

1. 0-1000°F in 6 hrs, then hold for 4 hrs.
2. 1000-12000°F in 5 hrs, then hold for 3 hrs.
3. 1200-1310°F in 5 hrs, hold for 50 hrs.
4. 1310-1200°F in 3 hrs.
5. 1200-1150°F in 0.5 hrs.
6. Then cool to room temperature in air.

The process was similar for the other steels.

4.4.3 Microstructures, Composition and Hardness of the steels

The hardness and the composition of the steels are examined in this section. The compositions of the bars are as shown in table 4.1 and 4.2.

Table 4.1: Composition of the hot-rolled steels used in the testing (All in wt%)

	C	Mn	P	S	Si	Ni	Cr	Mo	Cu	Sn	Al	V	B	Ti
1018	0.208	0.702	0.015	0.026	0.212	0.069	0.133	0.018	0.258	0.011	0.020	0.003	0.001	0.004
1045	0.476	0.744	0.011	0.037	0.273	0.051	0.077	0.015	0.109	0.004	0.037	0.004	0.000	0.005
1070	0.684	0.780	0.013	0.024	0.215	0.042	0.165	0.016	0.046	0.006	0.020	0.000	0.000	0.004

Table 4.2: Composition of the spherodized steels used in the testing (All in wt%)

	C	Mn	P	S	Si	Ni	Cr	Mo	Cu	Sn	Al	V	B	Ti
1018	0.160	0.828	0.010	0.028	0.193	0.014	0.079	0.011	0.053	0.004	0.020	0.001	0.000	0.001
1045	0.476	0.744	0.011	0.037	0.273	0.051	0.077	0.015	0.109	0.004	0.037	0.004	0.000	0.005
1065	0.640	0.800	0.014	0.010	0.280	0.070	0.150	0.020	0.130	0.009	0.024	0.002	0.000	0.002
1095	0.887	1.024	0.019	0.025	0.309	0.145	0.316	0.141	0.156	0.007	0.004	0.170	0.000	0.004

Figure 4.4 shows the photomicrographs of the microstructures. As one can see, the as-received steels showed a very pearlitic structure. For the spherodized steels, this lamellar cementite were transformed into spheroids by the spherodizing process. It is also evident that the cementite in the spherodized steels was not of a uniform size and this could have a role to play in the tool wear process. In particular, the 1095 steel showed a

very small cementite size, which was believed to be because it was vanadium killed [Table 4.2]. Figure 4.5 shows the hardness of the steels in various states.

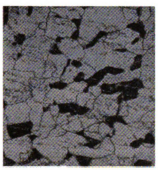

1018(as-received)

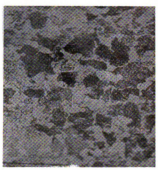

1045 (as-received)

1070(as-received)

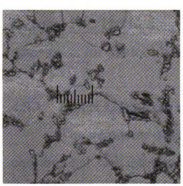

1018 (spherodized microstructure)

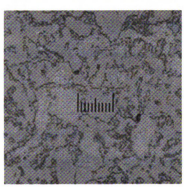

1045 (spherodized microstructure)

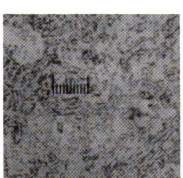

1065 (spherodized microstructure)

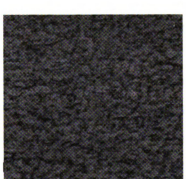

1095 (spherodized microstructure)

Figure 4.4: Microstructures of the steels used in the testing

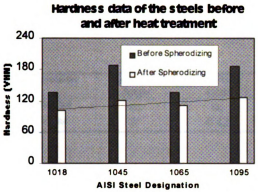

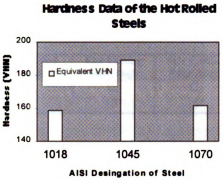

Figure 4.5: Hardness of the steels used in the machining tests

4.5 Inserts used in the experiments

The inserts for the experiments were procured on request from Kennametal, Inc., Latrobe, PA. The turning tool holder was also procured from them. Adequate number of spare parts for the tool holder were also purchased for exigencies during the experiment.

4.5.1 Insert Geometry and ISO/ANSI designation

The geometry of the inserts had the ISO designation SPGN 19 04 12. The integral chip breaker was intentionally avoided (1) to simplify modeling of tool temperatures, (2) to make an accurate measurement using the pyrometer and (3) to apply the 1-D ellipsoidal model. A large nose radius was chosen to avoid catastrophic failure of the insert and a large IC (Inner Circle diameter) was chosen to suitably place the pyrometer on top of the insert. It was felt that a proper choice of the nose radius is important since this could bring about chatter problems and difficulties in flank wear measurement if chosen improperly. It should also be mentioned that the depth of cut should be at least as high as the nose radius to have a suitable chip curl. There were also many opinions that the insert style was one of milling than turning. The inserts were used with a standard CSRPR 856D tool holder. The assembled tool signature of the insert, measured with the toolmaker's microscope is shown in table 4.3. Figure 4.6 illustrates the various geometric parameters.

Table 4-3 Cutting Tool Signature

Parameter	Back Rake Angle	Side Rake Angle	End Relief Angle	Side Relief Angle	End Cutting Edge Angle	Side Cutting Edge Angle	Nose Radius
Symbol	α_b	α_s	θ_c	θ_s	C_c	C_s	r
Value	0°	4°42'	4°42'	0°	15°	15°	3/64"

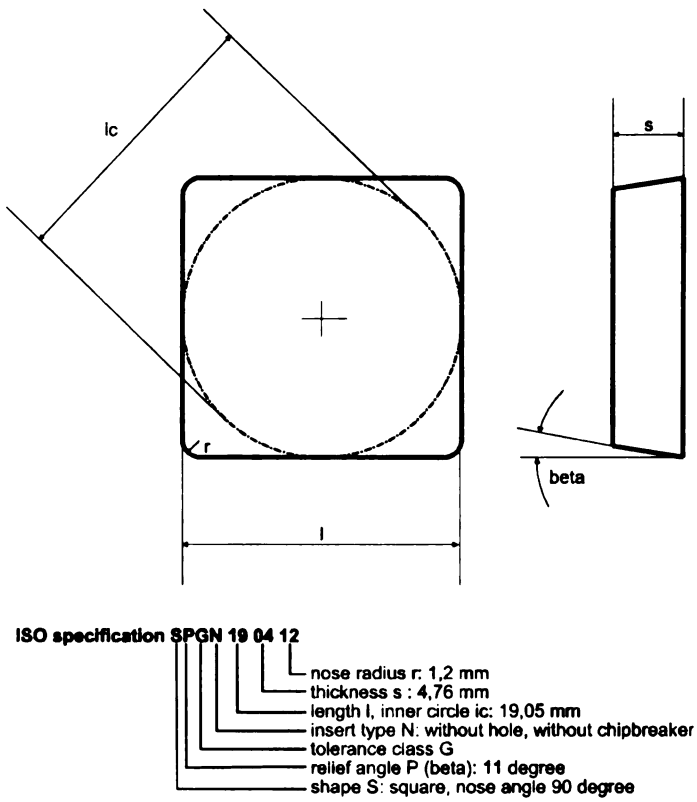

Figure 4.6: Illustration of the various geometric details of the cutting tool

4.5.2 Grade of substrate used

The substrate was a K420[2] grade, which consists mainly of WC and a Co binder has a slight alloying of TiC and TaC. The American standard for the same is C6-C7. The details are shown in table 4.4 [31]. Thermophysical properties of the grade collected from Santhanam [32] are shown in table 4.5. It has a medium binder content and a large grain size meant for general purpose steel machining. It is also renowned for the right balance of wear resistance and toughness.

Table 4.4: Properties of the substrate

K420		
ISO Specification	**Nominal Specifications**	
P25-P35	Porosity	A04-B00-C00
M25-M30	WC (Gsum)	1-8μm
Nominal Composition – wt%	HRA	91.2
Co 8.5	Hc(Oe)	140
TaC 10.9	Dens. (g/cc)	12.65
TiC 7.4	TRS (Mpa)	2170
WC 73.2		

Table 4.5: Thermophysical property data of substrates

Composition	Grain size	Hardness HRA	CTE μm/m°C	Thermal Conductivity W/m.K	Density g/mm²	TRS MPa
94WC-6Co	Fine	92.5-93.1	5.9	108	15.0	1790
94WC-6Co	Medium	91.7-92.2	5.4	100	15.0	2000
90WC-10Co	Fine	90.7-91.3	6.0	80	14.6	3100
72WC-8TiC-11.5TaC-8.5Co	Medium	90.7-91.5	6.8	50	12.6	1720

[2] Courtesy Kennametal, Inc.

4.5.3 Coating Materials and related details

The TiN coating was commercially available from Kennametal as KC710[2]. It consisted of the K420 substrate with a 4μm coating of PVD TiN over it. The two other coatings TiCN and Al_2O_3 were custom made for this study as follows. Uncoated inserts were sent to Balzers, Inc, Lansing, MI, where a 3.5μm coating of TiCN was performed. The PVD process used for this purpose was Reactive Ion Plating. Uncoated inserts were also sent to Valenite, Inc., Troy, MI, where a 3μm CVD coating of Al_2O_3 was performed. Due to the well-known problems of the Al_2O_3 coating adhering to carbide substrate [32], a 1μm intermediary layer of TiN was deposited between the Al_2O_3 and the carbide substrate. The nature of the CVD process used was not disclosed. The hardness data of the coatings was also collected from the literature and a variety of sources to be elaborated later on. The TiN coating was a golden colored coating whereas the TiCN had a bluish gray color and the Al_2O_3 coating had a dark black color. Also the TiN and TiCN coatings were shiny while the Al_2O_3 coating was rough and dull. This great difference in colors and texture persuaded the thin black coating in the temperature measurement as explained before.

4.5.4 Designation for the identification of the inserts

Given the huge volume of tests that were performed, it was imperative that a proper designation system for the inserts be evolved. This was done and the same designation used for the data sheets, the temperature records and the crater photographs stored on the computer. Figure 4.7 illustrates a sample naming scheme used. Tables 4.6 and 4.7 show the process parameters of the cuts with reference to this naming scheme. In all 84 cuts were performed, of which, two were invalid.

---

[2] Courtesy Kennametal Inc.

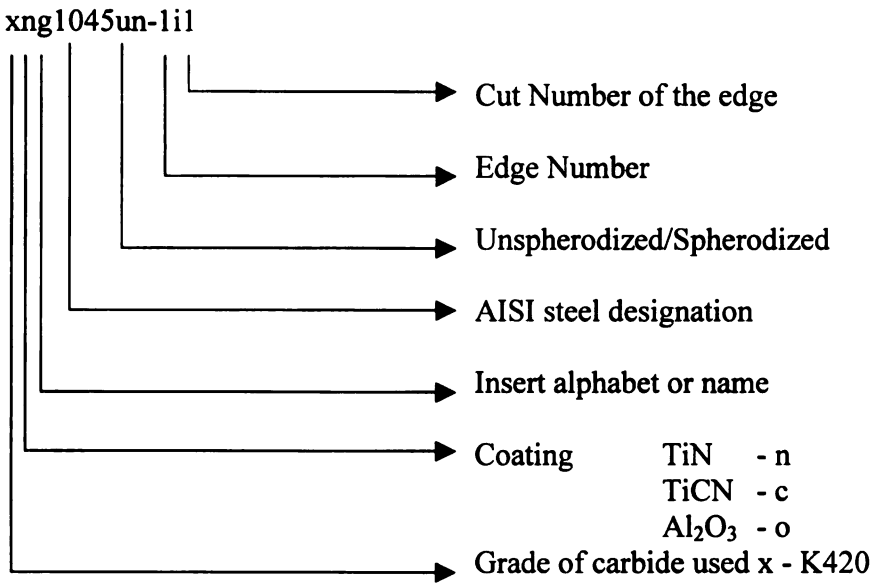

Figure 4.7: Sample-naming of the TiN insert used on AISI 1045 (spherodized) for the low speed cut.

Table 4.6: Process Parameters for the spherodized steels testing

Insert Designation	Work Material	Coating Material	Cutting Speed (m/min)	Insert Designation	Work Material	Coating Material	Cutting Speed (m/min)
	1018(sp)	TiN			1065(sp)	TiN	
xnf1018sp-1			99.29	xnh1065sp-1			103.18
xnf1018sp-2			164.30	xnh1065sp-2			170.22
xnf1018sp-3			239.57	xnh1065sp-3			219.21
xnf1018sp-4			274.09	xnh1065sp-4			261.37
		TiCN				TiCN	
xca1018sp-1			101.32	xcc1065sp-1			103.88
xca1018sp-2			164.05	xcc1065sp-2			157.73
xca1018sp-4			215.81	xcc1065sp-3			218.50
xca1018sp-3			274.44	xcc1065sp-4			241.14
		Al_2O_3				Al_2O_3	
xoa1018sp-1			102.06	xoc1065sp-1			105.56
xoa1018sp-2			164.54	xoc1065sp-2			157.66
xoa1018sp-4			207.55		Third cut with Al_2O_3 on 1065(sp) invalid.		
xoa1018sp-3			292.08	xoc1065sp-4			257.82
	1045(sp)	TiN			1095(sp)	TiN	
xng1045sp-1			100.08	xni1095sp-1			104.24
xng1045sp-2			162.36	xni1095sp-2			168.79
xng1045sp-3			225.68	xni1095sp-3			231.48
xng1045sp-4			289.04	xni1095sp-4			277.21
		TiCN				TiCN	
xcb1045sp-1			100.87	xcd1095sp-1			105.04
xcb1045sp-2			164.33	xcd1095sp-2			170.14
xcb1045sp-3			227.44	xcd1095sp-3			231.48
xcb1045sp-4			291.11	xcd1095sp-4			279.45
		Al_2O_3				Al_2O_3	
xob1045sp-1			100.14	xod1095sp-1			107.73
xob1045sp-2			164.92	xod1095sp-2			171.11
xob1045sp-3			227.88	xod1095sp-3			234.40
Xob1045sp-4			292.11	xod1095sp-4			274.74

Table 4.7: Process Parameters for the unspherodized steels testing

Insert Designation	Work Material	Coating Material	Cutting Speed (m/min)	Insert Designation	Work Material	Coating Material	Cutting Speed (m/min)
	1018(unsph)	TiN			1070(unsph)	TiN	
xnl1018un-1			90.90	xnn1070un-1			90.30
xnl1018un-2			154.40	xnn1070un-2			152.30
xnl1018un-3			214.30	xnn1070un-3			214.50
xnl1018un-4			275.60	xnn1070un-4			272.40
		TiCN				TiCN	
xcl1018un-1			91.00	xcn1070un-1			92.00
xcl1018un-2			153.00	xcn1070un-2			152.80
xcl1018un-3			214.00	xcn1070un-3			214.00
xcl1018un-4			275.70	xcn1070un-4			271.90
		Al_2O_3				Al_2O_3	
xol1018un-1			92.00	xon1070un-1			92.90
xol1018un-2			153.30	xon1070un-2			152.50
xol1018un-3			214.80	xon1070un-3			213.50
xol1018un-4			275.30	xon1070un-4			275.00
	1045(unsph)	TiN					
xnm1045un-1			91.60				
xnm1045un-2			164.30				
xnm1045un-3			221.90				
xnm1045un-4			274.50				
		TiCN					
xcb1045sp-1			91.60				
xcb1045sp-2			152.60				
xcb1045sp-3			220.60				
xcb1045sp-4			276.70				
		Al_2O_3					
		First cut interrupted due to BUE					
xob1045sp-2			152.20				
xob1045sp-3			221.00				
xob1045sp-4			284.10				

4.6 Area Measurement

Photographs of the crater were taken with a LECO SZH stereo microscope with a LECO 2001 image analyzer. Samples of the photographs taken are shown later in figure 5.4. Measurement of chip-tool contact area, which is a vital input in the inverse temperature estimation, posed a great challenge. After attempting a number of methods, it was found that it was most accurately measured using an image processing software. However, the spatial calibration was a critical issue. Figure 4.7 shows the methodology used in this regard. The diagonal formed by the ends of the nose radius was the easiest and the most accurate dimension, available right on the insert specimen. It also avoids any parallax error, if any. The image processing software also enabled adjustment of the contrast of the image. This was important since precise demarcation of the chip-tool contact area was sometimes absent.

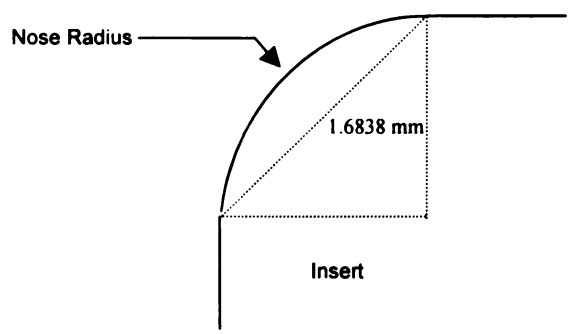

Figure 4.8: Illustration of the method for the area calibration

4.7 Tool Wear Measurement : set-up for Flank and Crater Wear

Flank wear was measured using the Mitutoyo TM-505 toolmaker's Microscope at a magnification of 200. The microscope was equipped with digimatic heads enabling measurements accurate up to 1μm. The set-up is shown in figure 4.8. Crater wear >5μm was measured on the stage and the optics of the microscope at a magnification of 30, with the Fowler D1040 Digital Test Indicator. The accuracy on this was 1μm. The calibration was checked using one-tenth thousandths gage blocks. For very shallow craters, the Sloan

Dektak IIA surface profilometer in the premises of the Physics Department of M.S.U. was used. A sample of the profiles obtained is shown in figure 4.9.

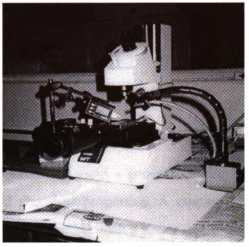

Figure 4.1: Set-up on the TMM for measuring flank and crater wear

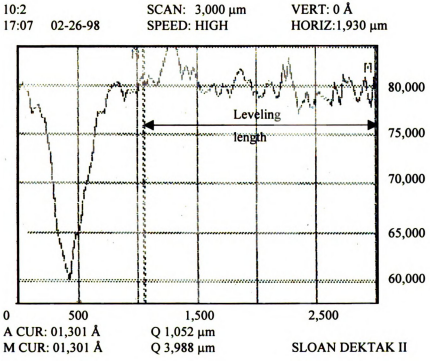

Figure 4.2: Sample of crater profiles (Cut-ID xoa1018sp-2)

Chapter 5

RESULTS AND DISCUSSIONS

5.1 Results of the Computer Algorithm

The results of the computer algorithm [Appendix A] yield a general ranking of the three candidate coatings from the hardness and chemical properties. A coating with a greater hardness has a better abrasion resistance and a coating with a lower free energy of formation has a greater resistance to chemical dissolution. Though cementite is softer than the coating materials at all temperatures, the variation of the abrasive wear-rate with temperatures, as given by the theoretical formulae in Chapter 2 was more keenly seen.

Interestingly, 3-body abrasion showed a decreasing rate with temperature. This is justified since even in the work of Rabinowicz [33,24], a rapid fall in wear-rate was observed with decreasing hardness of the abrasive. Two-body abrasion, however, shows an increasing rate with temperature, simply because the hardness of the abrasive is assumed to be infinite at all temperatures and only softening of the tool material is taken into account. From a practical standpoint, the validity of this assumption is indeed questionable.

Dissolution, being inherently a thermally activated mechanism, increases steeply with temperature. The exact methodology of the numerical computation is elaborated in Appendix A. Figures 5.1 and 5.2 show the output of the computer program for the three coatings in absolute terms.

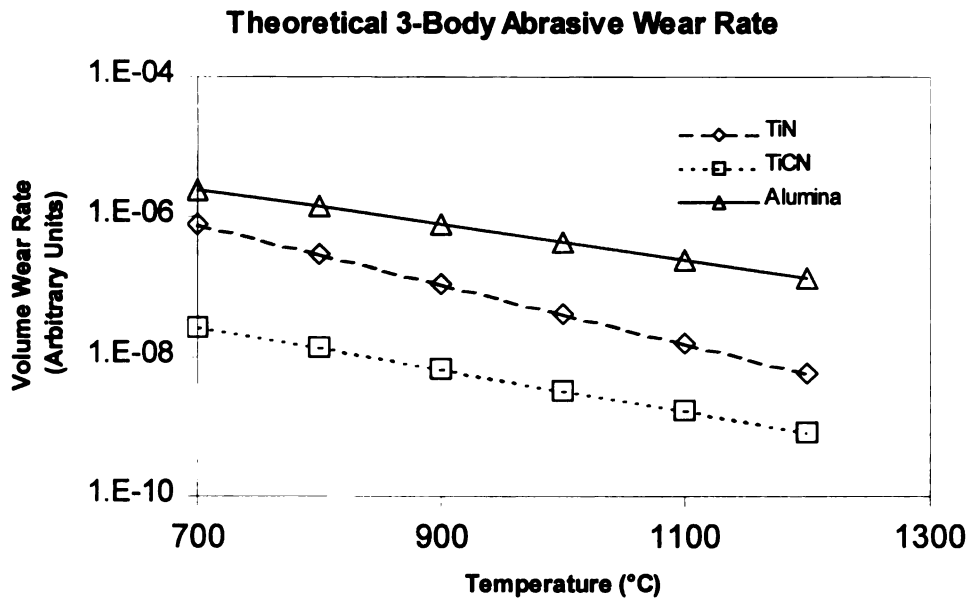

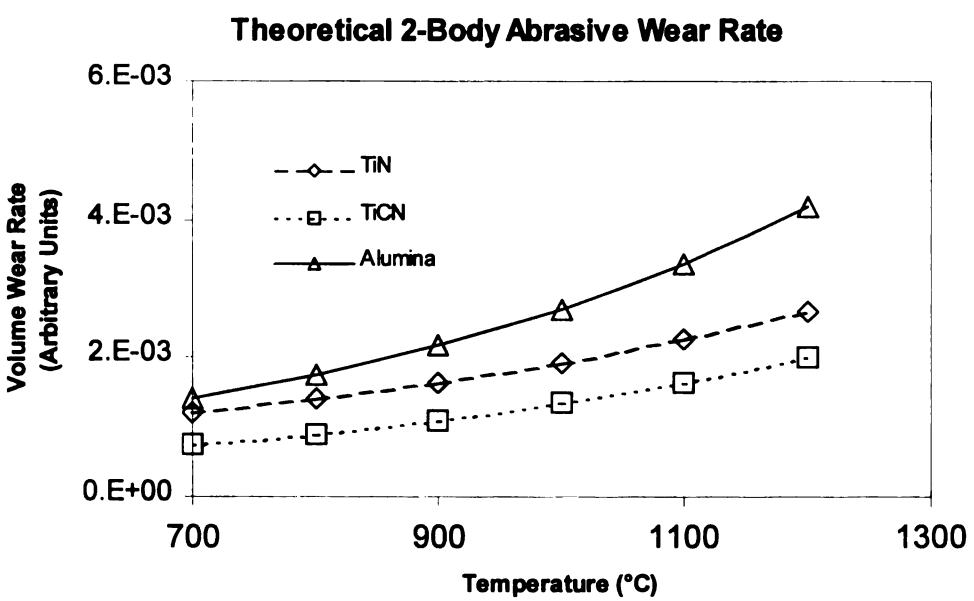

Figure 5.1: Charts illustrating the ranking of the coatings for the two abrasive wear mechanisms.

5.1.1 Abrasive Wear

It can be seen in figures 5.1 and 5.2 that wear-rate decreases with temperature for the 3-body abrasive wear model whereas it increases with temperature for the 2-body wear model. A curve fitting of the form $Ae^{\alpha T}$ was performed for figure 5.1 for prediction of wear with the experimental results. The final equations evolved for the 6 cases are shown in table 5.1.

Table 5.1: List of Wear-rate Equations for the calibration purpose
(T in °C, w.r. stands for wear per sliding distance)

Coating Compound	Three-body Wear Equation	Two-Body Wear Equation
TiN	$w.r. = 7.5506E\text{-}04e^{-9.8077E\text{-}03\,T}$	$w.r. = 3.9173E\text{-}04e^{1.5962E\text{-}03\,T}$
TiCN	$w.r. = 3.6295E\text{-}06e^{-7.0089E\text{-}03\,T}$	$w.r. = 1.8166E\text{-}04e^{2.0011E\text{-}03\,T}$
Al_2O_3	$w.r. = 1.3742E\text{-}04e^{-5.7516E\text{-}03\,T}$	$w.r. = 3.0735E\text{-}04e^{2.1740E\text{-}03\,T}$

5.1.2 Dissolution Wear

As can be seen from figure 5.2, dissolution wear-rate increases with temperature. Also, Al_2O_3 is considerably more inert that the other two coatings. This corresponds to the common experience of using Al_2O_3 coatings for finish machining since higher temperatures are encountered due to the high cutting speeds employed for finishing. The curves were then fitted in the form Ax^n, where x is the temperature in °K. The reason for using this form was the steep drop in dissolution wear with decreasing temperature. The final equations are shown in table 5.2.

Table 5.2 Curve fitted relations for the dissolution wear of the coating materials (x is temperature in °K, w.r. stands for wear per unit time)

Coating	Dissolution Wear Equation
TiN	$w.r. = 1.1658E\text{-}54x^{1.6284E+01}$
TiCN	$w.r. = 1.3575E\text{-}42x^{1.2528E+01}$
Al_2O_3	$w.r. = 8.1920E\text{-}96x^{2.8201E+01}$

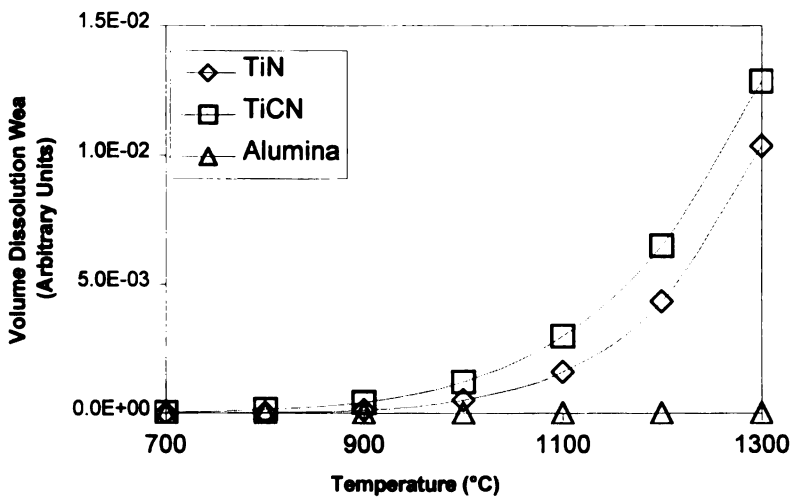

Figure 5.2 Figure illustrating the ranking of the coatings for the dissolution wear mechanism.

5.2 Temperature trends with cutting speed

A sample of the temperature profiles for the cuts on spherodized steels, TiN coated K420 while machining spherodized AISI 1095 steel, is shown in figure 5.3. One can note an increasing trend with cutting speed. The curve fitting, to obtain the steady state cutting temperature, is explained in Appendix D is shown in the same graph.

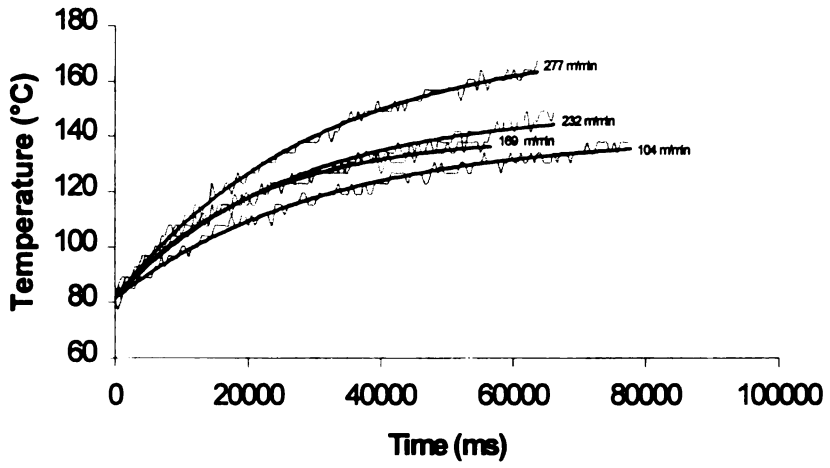

Figure 5.3 Temperature records of cuts on AISI 1095 steel with TiN coated K420 carbide
(Curve fitting process shown alongside)

Although the pyrometer technique was easy to conceive and implement, the accuracy in measurement had to be validated with the data obtained in the past. The chip-tool interface temperature measurements compared favorably with the results obtained by Subramanian *et al.* [20] who employed the same work material, similar cutting conditions and grade of carbide. They had estimated the interface temperatures based on the cutting forces of Boothroyd's model [30]. The flank temperatures observed in the present experiments showed an increasing trend with the cutting speed, except in a few cases [Appendix C]. Complications due to abnormally large contact areas may have contributed to the high temperatures observed in these low speed cuts. Another possible reason could

be that the peak temperature was far removed from the cutting edge thereby decreasing the apparent distance of the pyrometer to the interface.

The inaccuracies in the inverse temperature estimation schemes such as the 1-D ellipsoidal model is fortunately low since the variation in the temperature field in the chip-tool interface is mitigated at the far field by the dampening of higher spatial temperature frequencies by the tool body [26]. Though the curve fitted peak temperature based on pyrometer readings [See Appendix D] generally increased with cutting speed as shown in figure 5.3, there were many instances where the pyrometer did record lower temperatures at higher speeds. The reason suggested is that the interface temperature in the inverse estimation was a function of both the pyrometer temperature and the contact area (which showed a decreasing trend as explained in the following section). This is direct evidence of the presence of steep temperature gradients in the cutting tool during cutting since this implies that the temperature of the area of heat input into the tool is far higher than the temperature outside this region. From the argument of the ellipsoidal model, this stands justified since, the volume for heat removal is higher farther away from the tool [figure 3.2], and hence represents a greater capacitance for storage of heat.

The trends of the rake face temperature with cutting speed for the as-received (normalized) steels were not as uniform as that obtained with the spherodized steels [Appendix C]. The pearlitic structure of the steel, which represents a lower mean-ferrite path [25], could have made the flow characteristics of the steel substantially different from that of the spherodized counterpart. The undetermined pre-work in the steel could have also influenced the chip-tool interface temperature.

5.3 Contact Area Trends

A significant finding in the results [Appendix C] was that *the chip tool contact area* showed a decreasing trend with cutting speed in both the spherodized and unspherodized cases. Subramaniam *et al.* [20] observed an increase in the *crater area* with cutting speed. The difference between the chip tool contact area and the crater area is that while

the chip-tool contact area corresponds to the region of heat input into the tool and the area of partial or complete seizure [40], the crater area corresponds to the amount of coating and substrate material carried away by the chip. The contact length was similar among the various coatings, which was also observed by Dearnley [9]. As is evident from figure 5.4, crater wear commences sooner at a higher cutting speed, possibly due to the chemical inertness and the resistance to surface traction offered by the coating material at lower speeds. It can also be noted that the alumina coating did not wear as much as the other coatings at the same cutting speed Considering the remarkable chemical inertness of Al_2O_3 [7], this elucidates the thermo-chemical component of crater wear.

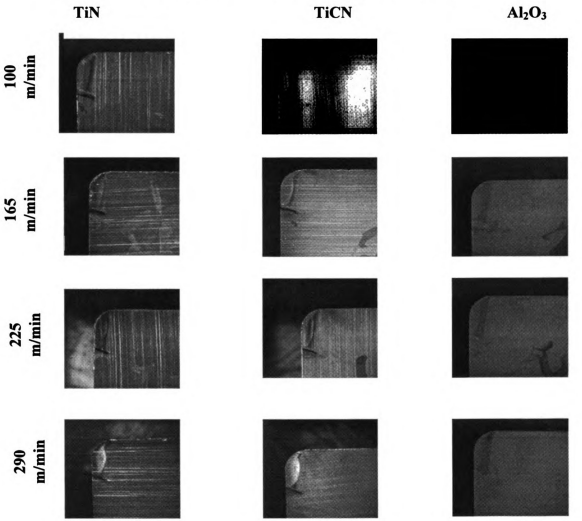

Figure 5.4: Photographs of K420 carbide coated with TiN, TiCN and Al_2O_3 respectively after machining spherodized AISI 1045 steel at increasing cutting speeds at f = 0.356 mm/rev and d.o.c = 1.905 mm.

Among the various work materials investigated, the chip-tool contact area showed a slightly decreasing trend with carbon content of the steel. The contact area is conjectured to be a strong function of the fracture toughness [Appendix C] of the work material, since this property governs the deformability at the shear zone.

5.4 Flank Wear

Flank wear has widely been recognized as the most appropriate criterion for tool life [11]. Chubb and Billingham [15] found that the removal of the coating in the region of the flank could accelerate the rate of wear. Hence, the resistance of a coating in the progression of flank wear deserves greater attention. Dearnley [9] and Cho and Komvopoulos [10] concluded that the WC phase in the substrate is prone to dissolution into α or γ phases of steel and dissolution wear supercedes any other mechanism of wear for the case of uncoated carbide grades without any TiC or TaC alloying [13].

In the present work, as expected, the flank wear-rates increased with the cementite content of the steels. As noted by Kim and Durham [17], the region of the flank wear could be divided into several zones of damage which includes the zone reminiscent of superficial plastic deformation and plowing by small carbide grains [10]. In this study, flank wear was measured at the region of wear land exhibiting uniformity in wear pattern. Ramalingam and Wright [2] had noted that alloy chemistry does not satisfactorily explain the machinability of steel since nominally identical alloys yield different machinabilities in different heats. Thus, it has been corroborated herein that the constitution of the steel in terms of its hard and soft phases is responsible for flank wear and hence its machinability. Abrasion by other means (such as the wear debris generated by the tool) cannot give rise to a uniform wear pattern since this form of abrasion is stochastic in nature.

The effect of competition between the various mechanisms in coated tools is the problem at large and requires careful introspection. It was seen in the present work that the Al_2O_3 coated inserts showed scouring marks uniform in length from the cutting edge

[Figure 5.5] while the other coated inserts showed scouring marks but with a shiny band where the carbide substrate was exposed. It can also be seen in Appendix C that TiCN coating showed the lowest wear-rate. In the context of coated tools, it is common experience that coated tools exhibit a lower crater wear-rate due to the impedance to solid solution formation offered by the coating. Given these facts, the superior chemical inertness of Al_2O_3 [7] and the higher hot hardness of TiCN [31], it can be concluded that temperatures prevalent at the flank do allow preferential dissolution of WC to take place but the *progression* of flank wear is resisted by the mechanical superiority of the coating. This resistance is a property greatly determined by the hardness of the coating at the flank temperature.

It should be noted that the preceding arguments would be true only if abrasion is the predominant mode of mechanical wear. This may not hold if more complex phenomena such as thermal cracking, mechanical fatigue cracking, chipping or fracture start adding to the damage of the cutting tool.

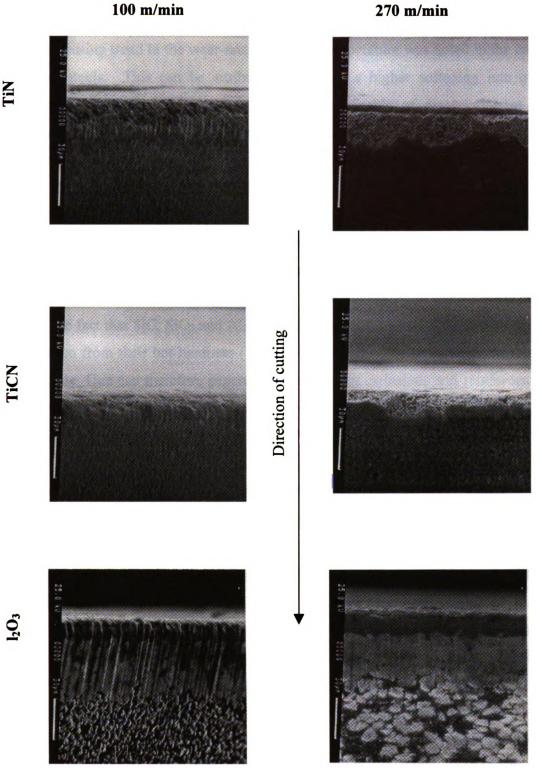

Figure 5.5: SEM micrographs (800×) of the worn flank surfaces of the coated cutting tools after machining spherodized AISI 1045 steel for low and high cutting speeds.

In the overall analysis, the TiCN coating showed the highest resistance to flank wear. A decreasing trend in the wear-rate with flank temperature was noted in the case of spherodized steels. This can be attributed mainly to a higher softening rate of the abrasive particles. Suh [19] mentions that Fe_3C is capable of dissociation at high temperatures, vis-a-vis oxide and nitride inclusions. This is also a possible reason for the decrease in wear-rate with temperature, though not quantitatively ascertained. In particular, the alumina coating exhibited the greatest sensitivity to flank wear due to a higher softening rate [7] reflecting the contrasting properties of the Al_2O_3 and the TiCN coatings. While Brun *et al.* [4, Section 1.2 (paragraphs 2,3,4)] had observed excessive wear-rates while machining silica reinforced aluminum and the same was the case with Ramalingam and Wright [2], wear was tolerable in the machining of plain carbon steels. In view of the fact that SiC, SiO_2 and Al_2O_3 are more refractory materials than cementite, as can be seen from their hot hardness [7], they can inflict a greater damage on the tool than cementite. One can therefore generally conclude that inclusions and reinforcements in a material should be chosen so that they strengthen the material but do not degrade machinability at higher temperatures encountered in high speed machining.

The final part of the analysis is an attempt to calibrate the comprehensive wear equations for the three coatings. Figure 5.6 shows the relevant graphs for the flank wear trends for three coatings. As can be seen from the figure 5.6, there is a convincingly decreasing trend in the spherodized steels and a moderately increasing trend with the unspherodized steels. The increasing trend in the case of the latter can be mainly attributed to the fact that the cementite particles are firmly rooted in the ferrite matrix. This supports modeling of the former with the three-body model and the latter with the two-body wear model. The decreasing trend should not give the notion that flank wear decreases with cutting temperature, rather, the rate of damage on the flank decreases with cutting temperature. The trends are not clearly evident with TiCN since the hard coating [31] was impervious to flank wear, due to the inadequate duration of the cuts. This testifies to the fact that abrasion is the rate-controlling mechanism on the flank.

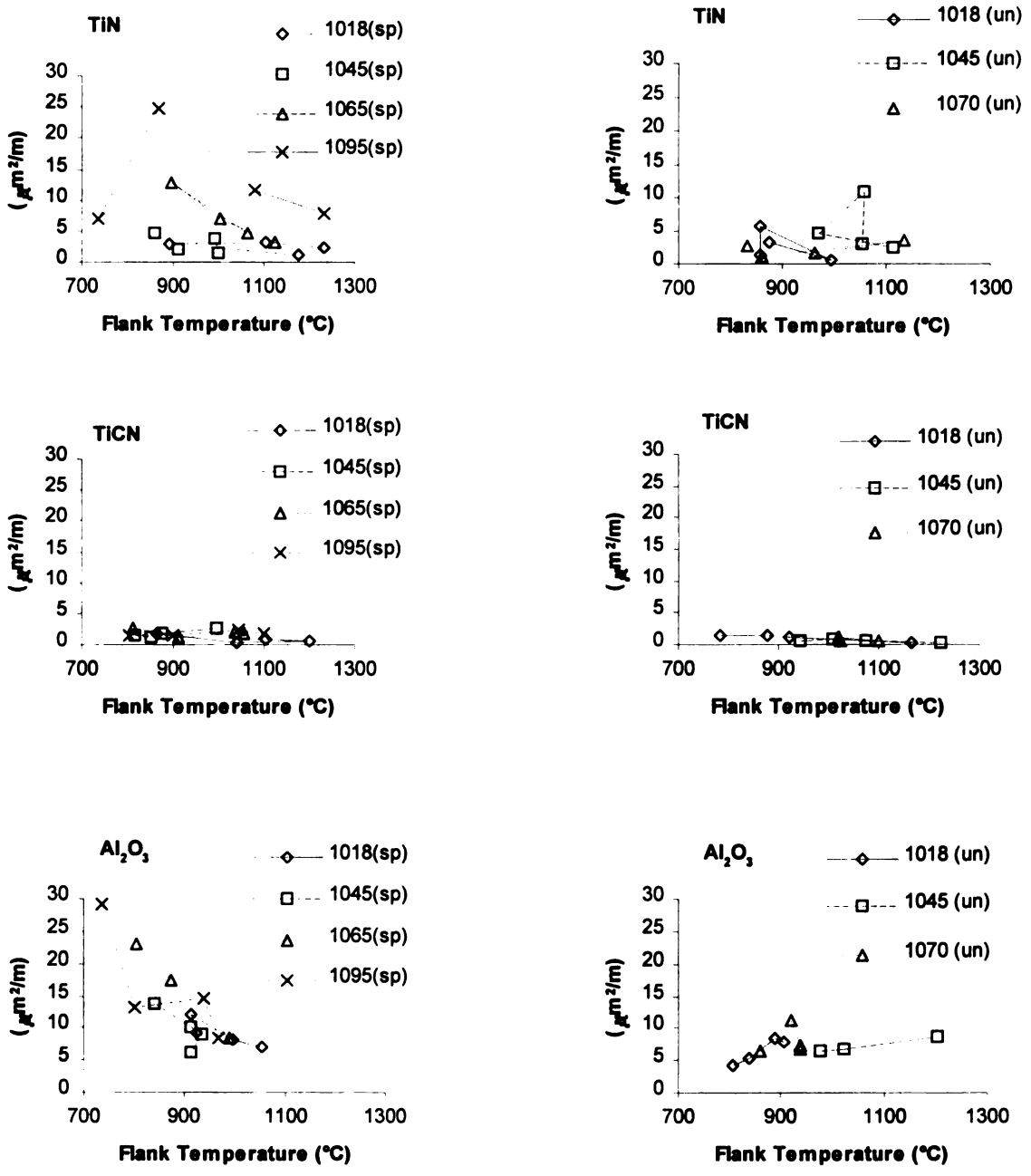

Figure 5.6: Plots showing the variation of the volume flank wear per sliding distance for the three coating materials. (sp-spherodized steel, un-unspherodized steel)

5.5 Crater Wear

Crater wear on coated inserts presents an interesting topic for investigation. An increasing trend [Figure 5.7] was noted in most cases. The general pattern of wear on the rake face consisted of a central region where the carbide substrate is exposed and a peripheral area where the coating seemed to resist removal by the flowing chips [Figure 5.4]. Crater wear in coated inserts is pronouncedly lesser than in uncoated carbides. It is therefore doubtful as to whether the same criteria for tool life [1] can be employed, and hence, suitable amendments are needed for a tool life criteria for coated cutting tools. It is speculated that there is a connection between the erratic nature of the rake face topography in coated tools, as observed in this study, unlike uncoated tools, to the wide variation in tool life of coated tools noted by Chubb and Billingham [15]. It was also found that the point of greatest depth on the crater was 500-700μm away from the cutting edge implying that the peak temperature occurred in the vicinity of this point. Moreover, the variation in the texture from the smoothly worn carbide substrate to the parental roughness of the coating suggested a wide range for the temperature on the rake face.

An explanation for the dependence of crater wear with cementite content can be elicited from the preceding point. Dissolution wear has no particular relation to the cementite content in the steel. That being the case, what was the reason for the increasing trend in the crater wear-rate with carbon content in the steel [Figure 5.7], if dissolution was the rate-controlling mechanism on the rake? A closer examination of the rake face revealed that the depth of the crater was somewhat proportional to the width of the crater. It can therefore be concluded that, at the periphery of the crater the coating was being abraded, whereas at the center of the crater, the exposed substrate was being dissolved continuously. Hence abrasion brought about the widening of the crater exposing a greater part of the substrate and dissolution brought about the deepening of the crater. This justifies the need for both abrasion and dissolution in the quantitative modeling of crater wear. It is suggested that in the design of multi-layered coatings, the outer layer be a coating resistant to abrasive wear and the intermediary layer be one resistant to dissolution.

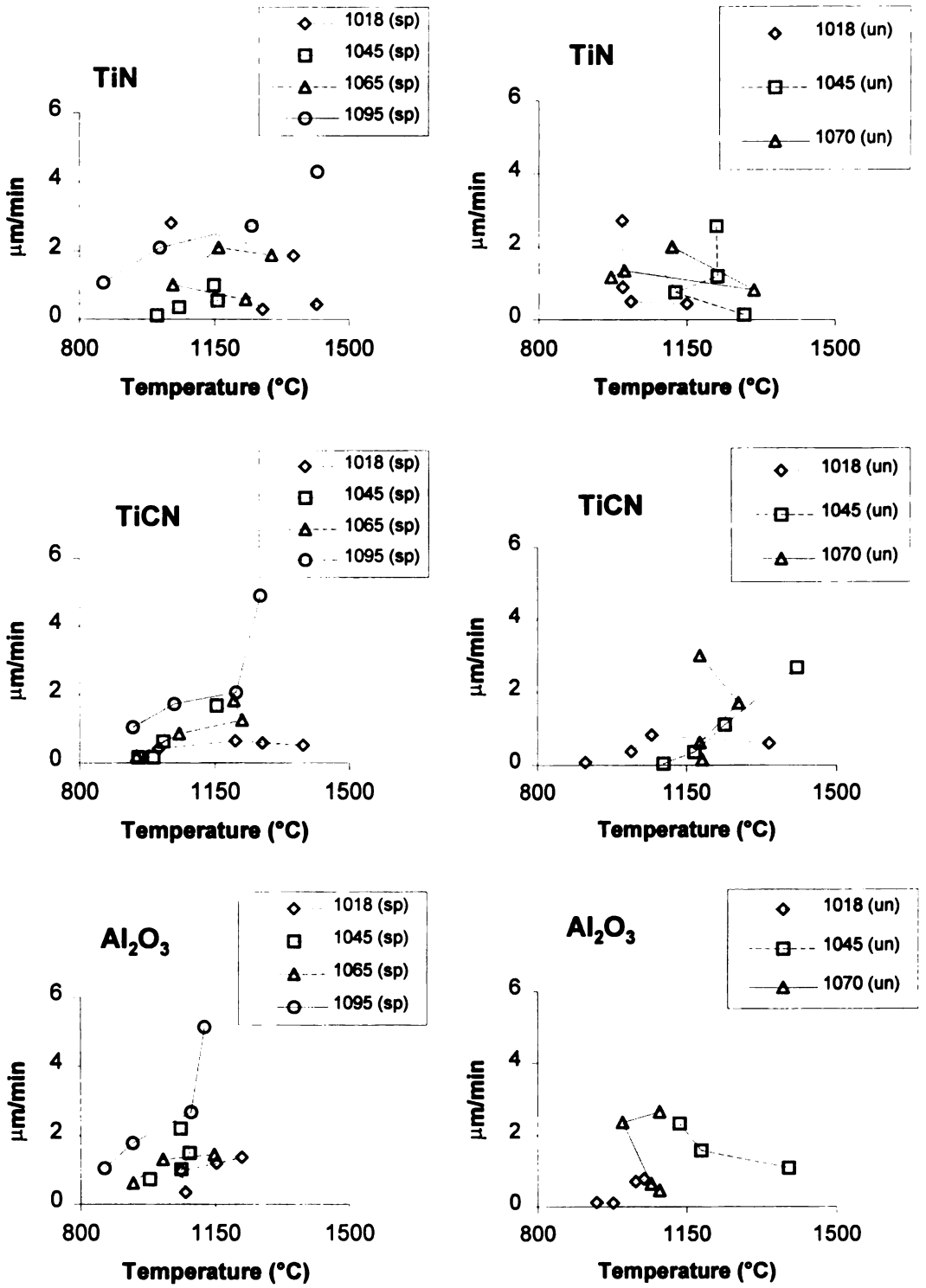

Figure 5.7 Plots showing the variation of the crater wear-rate for the three coating materials. (sp-spherodized steel, un-unspherodized steel)

5.6 Calibration

With use of the equations in tables 5.1 and 5.2 one can obtain a calibration for the wear-rates based on equations 2.6 and 2.7 and hence values for the constants A and B. As a recapitulation, the value for 'A' has to be obtained for flank wear, since it is dominated only by abrasion and both 'A' and 'B' for crater wear since both mechanisms operate. Further, for flank wear, it should be remembered that the three-body wear mechanism is assumed to operate in the machining of spherodized steels whereas the two body mechanism is assumed to operate in the machining of unspherodized steels. Furthermore, in the case of abrasion on the crater only the three-body mechanism is assumed to operate, since temperatures are excessively high for the abrasive to retain any hardness. The details of the governing relations of the wear mechanisms were explained in Chapter 2.

As an example, calibrations for Al_2O_3 for flank wear and crater wear while machining spherodized steels is illustrated in figure 5.8. This was performed on the software SigmaPlot®. The values are listed in Appendix C. Figure 5.9 shows the plot of the constants 'A' and 'B' obtained from the calibration process. There is a general agreement in the trends of the models and that of the experimental results, however, it was not impressive for the as-received steels probably because of the pre-work in the steels and presence of distributed hard spots, which injure the tool in an arbitrary fashion.

Since 'A' and 'B' are quite different in their order of magnitude, they are plotted on a logarithmic scale in figure 5.9 for visualization purposes. It can also be observed in figure 5.9 that the values for individual 'A's and 'B's are within the same order of magnitude. This is promising since this substantiates the correctness of the modeling, despite the fact that only one cut was taken for each machining condition.

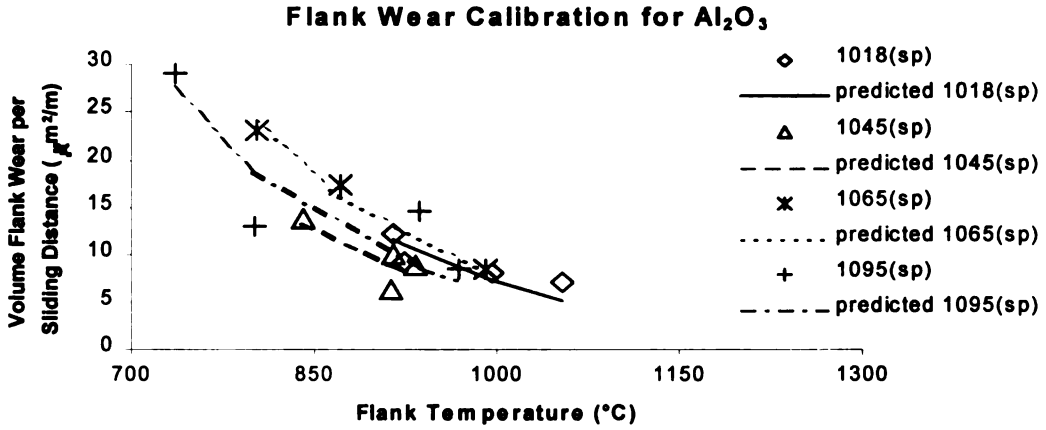

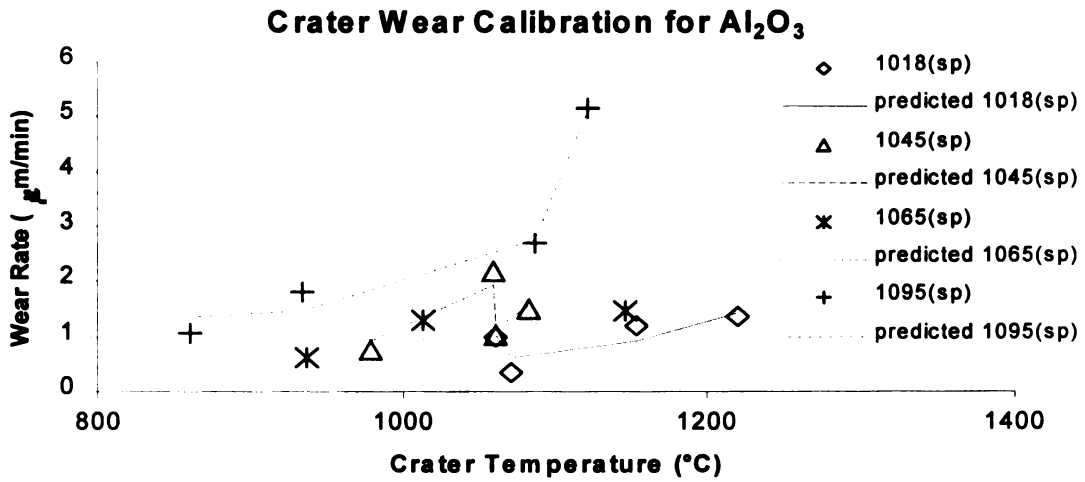

Figure 5.8: Plot of the predicted and the experimental wear data for Al_2O_3 while machining spherodized steels

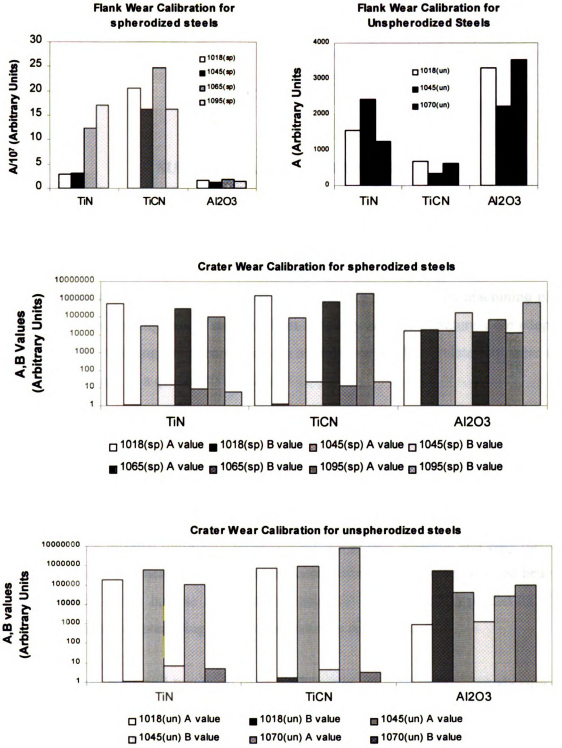

Figure 5.9: Plots of the constants obtained from the calibration process.
(sp - spherodized steel, un – unspherodized steel)

Chapter 6

SUMMARY AND CONCLUSIONS

The following summarizes the work performed: -

Wear of the flank and the crater of coated carbide tooling while machining plain carbon steels was investigated. Wear models in tribology and the literature were adopted in modeling and studying the phenomena. An attempt was made to relate tool wear and cutting temperatures in a quantitative fashion.

The infrared pyrometry technique was utilized in the measurement of rake face temperature. The 1D ellipsoidal scheme of Yen and Wright [44] was used in the inverse estimation of the chip-tool interface temperature. Oxley's recipe for the flank temperature was adopted. The dependence of interface temperatures was on the process parameters was studied. The infrared pyrometry technique proved to be a versatile and easy method enabling easy measurement of the rake face temperatures of the tool, but relied heavily on the accuracy of the inverse estimation schemes for its accuracy in prediction. The related problem of the interfering chips was effectively dealt with.

The three-body and two-body wear models were used for describing abrasion of the flank surface of spherodized and unspherodized steels respectively whereas the dissolution and the three-body wear models were used in obtaining a comprehensive description of crater wear in both steels. Recommendations for further developments in

tool materials such as multi-layered coatings and work materials include having an intermediary layer resistant to dissolution and an outer layer resistant to abrasion. The criteria for the predictability of tool wear have been outlined clearly. Reinforcements in a work material should be chosen so that they don't degrade the machinability of a material.

Among the major findings in this study are that steep gradients in temperature are present on the rake face of the cutting tool. Chip-tool contact area decreases with cutting speed. Contact area is proportional to the fracture toughness [Appendix C]. Flank and crater wear were found to increase with the cementite content in the steel. Spherodized steels showed a decreasing flank wear per sliding distance with temperature whereas hot-rolled, unspherodized steels showed a moderately increasing trend. Both types of steels showed an increasing rate of crater wear with temperature. Modeling of tool temperatures, which was undertaken, showed that there were steep temperature gradients in the cutting tool and temperatures depended on the area of heat input into the tool.

The appropriate conclusions drawn include affirming that abrasion was the rate-controlling wear mechanism in the wear of coated carbide tools while machining plain carbon steels, though preferential dissolution of the carbide substrate is also possible. Crater wear involved both abrasion and dissolution. The wear models used in tribology proved to be reasonably accurate in predicting wear rates on both the crater and the flank.

APPENDICES

Appendix A

COMPUTER ALGORITHM

A.1 The main part of mainprog.f

```
character coating*8,elea(6)*2,compound*8
        integer xa(6)


C       'coating' IS THE INPUT VARIABLE FOR THE COATING, 'elea' IS THE GLOBAL
C        ARRAY CONTAINING THE ELEMENTS OF THE COATING, READ FROM THE FILE COMP1.DAT
C       THERE ARE FIVE FILES IN ALL. MAINPROG.F WHICH IS THE MAIN PROGRAM FILE,
C       MECH1.DAT, WHICH CONTAINS THE HARDNESS DATA, CHEM1.DAT CONTAINS THE CHEMICAL
C       DISSOLUTION DATA AND ExFreeEn.dat WHICH CONTAINS THE EXCESS FREE ENERGY OF
C       SOLUTION OF  INDIVIDUAL ELEMENETS IN ALPHA IRON. THE PROGRAM CAN WORK
C       FOR AT THE MOST TERTIARY COATINGS. IN ORDER TO UPGRADE FOR MORE COMPLEX
C       COATINGS ON HAS TO JUST ADD STATEMENTS RELATED TO THE ELEMENTS IN THE 'elea'
C       ARRAY. ALSO, FOR NON STOICHIOMETRIC COATINGS ONE HAS TO ENTER THE NUMBERS WITH
C       AN INTEGRAL NUMBER OF ATOMS IN THE MOLECULE.

C       The following unit reads the file 'COMP1.DAT' for the compound
C       name and its elements.

C       INPUT COATING AND ITS DETAILS
        write(*,30)
30      format('What is the coating?')
        read(*,31) coating
31      format(A8)
        open(unit=2,file='COMP1.DAT',blank='ZERO',status='OLD')
52      read(2,53,end=68) elea(1),elea(2),elea(3),xa(1),xa(2),xa(3),compound
53      format(A2,A2,A2,I2,I2,I2,A8)
        if(compound.eq.coating) then
         goto 70
        else
        endif
        goto 52
68      write(*,69)
69      format('SORRY COATING IS NOT TO BE FOUND IN THE LIST')
        stop
70      close(2)
        call mechwear(coating)
        call chemwear(coating,elea,xa)
        end
```

A.1.1 Listing of 'subroutine mechwear'

```
C       THE FOLLOWING SUBROUTINE GENERATES THE MECHANICAL WEAR DATA FOR
C       THE COATING BASED ON THE HARDNESS OF THE ABRASIVE AND THE COATING.
C       BOTH TWO BODY AND THREE BODY WEAR DATA ARE GENERATED.
C       THE DECLARATIONS ARE AS FOLLOWS: -ctng STANDS FOR THE COATING.
C       ALL VARIABLES WITH 'COMP' ENDING DENOTE COMPOUNDS, ANY VARIABLE WITH
C       h IN IT DENOTES HARDNESS.THE HARDNESS OF
C       ANY MATERIAL CONCERNED IS EXPRESSED IN THE FORM H(T)=H0*EXP(-ALP*T). THIS
C       WOULD THEN REPRESENT THE SOFTENING IN THE MATERIAL AT A HIGHER TEMPERATURE. ALL
't's
```

```
C       REPRESENT TEMPERATURE. THE SUFFIX 'ref'STANDS FOR THE REFERENCE COMPOUND AND THE
SUFFIX
C       'ab' STANDS FOR THE ABRASIVE. TO CHANGE THE ABRASIVE FOR TEH MODEL ONE HAS TO
C       CHANGE THE FIRST ELEMENT IN THE MECH1.DAT FILE. SINCE THE HARDNESS OF A MATERIAL
C       MAY NOT ALWAYS BE EXPRESSIBLE IN THAT FORM, AN INTERMEDIATE TEMPERATURE
C       IS CHOSEN SO THAT FROM THAT TEMPERATURE ONWARDS, THE HARDNESS TAKES A
C       DIFFERENT FORM. HENCE THE TWO TEMPERATURES t1 AND t2.


        subroutine mechwear(ctng)
        character comp*8,refcomp*8,ctng*8,abcomp*8
        real h1,alp1,h2,alp2,refh1,refalp1,refh2,refalp2
        real ah1,aalp1,ah2,aalp2
        integer t1,t2,reft1,reft2,t,i,at1,at2,abrat
        real th,ah,refh,relwear,abrwearcoeff,twobodyrelwear,abrwearcoefftwobody

C       IN THE MECH1.DAT FILE, THE FIRST RECORD CORRESPONDS TO THE REFERENCE TOOL MATERIAL
C       FOR THE RELATIVE WEAR CALCULATION. THE SECOND CORRESPONDS TO THE ABRASIVE
PARTICLE.
C       HENCE THE ORDER OF DATA COLLECTION FROM THE FILE.


c       GETTING THE DATA FOR THE REFERENCE TOOL MATERIAL
        open(unit=2,file='MECH1.DAT',blank='NULL',status='OLD')
        read(2,500) refcomp
500     format(A8)
        read(2,510) refh1,refalp1,reft1
510     format(F7.1,F10.8,I4)
        read(2,520) refh2,refalp2,reft2
520     format(F7.1,F10.8,I4)

c       GETTING THE DATA FOR THE ABRASIVE MATERIAL
        read(2,521) abcomp
521     format(A8)
        read(2,522) ah1,aalp1,at1
522     format(F7.1,F10.8,I4)
        read(2,523) ah2,aalp2,at2
523     format(F7.1,F10.8,I4)
        close(2)

C       THE NEXT UNIT RELATES TO SERACHING THE DATA FOR THE CANDIDATE TOOL MATERIAL. AS
MENTIONED
C       BEFORE, HARDNESS IS EXPRESSED IN THE SAME FORM AS BEFORE. AGAIN FOR MORE
CORRESPONDENCE
C       WITH THE EXPERIMENTAL VALUES, THE HARDNESS FORMULA IS SPLIT INTO TWO REGIONS.

c       LOCATING THE HARDNESS DATA FOR THE T/M IN THE FILE
        open(unit=2,file='MECH1.DAT',blank='NULL',status='OLD')
525     read(2,530,end=560) comp
530     format(A8)
        read(2,540) h1,alp1,t1
540     format(F7.1,F10.8,I4)
        read(2,550) h2,alp2,t2
550     format(F7.1,F10.8,I4)
        if(comp.eq.ctng) then
         goto 580
        else
        endif
        goto 525
560     write(*,570)
570     format('SORRY ABRASION DATA NOT FOUND FOR THE TOOL MATERIAL')
        return
580     close(2)

C       THIS IS THE MAIN UNIT WHICH GENERATES THE WEAR DATA. AN OUTPUT FILE IS OPENED FOR
WRITING
C       AND HEADINGS ARE WRITTEN. A SEPARATE SUBROUTINE 'hardness' FOR THE HARDNESS
CALUCULATION USING THE
C       FORMULA IS WRITTEN. THAT WILL BE SEPARATELY EXPLAINED. APPROPRIATE ERROR MESSAGES
ARE
C       ALSO WRITTEN SIDE BY SIDE.
```

```
      open(unit=3,file='mechwear.out',blank='NULL',status='NEW')
      write(3,593)
593   format('Temperature(C)   Relative Abrasive wear    Two body relative wear
T/Hardness   A/Hardness  wear coeff(3-body)  Wear coeff.(2-body).')
      do 800 i=1,14
      t=(i-1)*100

      if(t.le.reft1) then
       refh=hardness(refh1,refalp1,t)
      elseif(t.le.reft2) then
       refh=hardness(refh2,refalp2,t)
      else
       write(*,600)
600    format('SORRY TEMPERATURE EXCEEDED FOR THE REF. MATL.:Termination')
       return
      endif

      if(t.le.t1) then
       th=hardness(h1,alp1,t)
      elseif(t.le.t2) then
       th=hardness(h2,alp2,t)
      else
       write(*,610)
610    format('SORRY TEMPERATURE EXCEEDED FOR THE T/M: Termination')
       return
      endif

C     THIS UNIT MEASURES THE ABRSIVE TEMPERATURE. AS SHOWN IN THE NEXT LINE A MODEST
ASSUMPTION
C     THAT THE ABRASIVE TEMPERATURE IS 90% OF THE INTERFACE TEMPERATURE IS MADE. THIS IS
AN
C     IMPORTANT POINT AND IS QUESTIONABLE.

      abrat=90*(i-1)
      if(abrat.le.at1) then
       ah=hardness(ah1,aalp1,abrat)
      elseif(abrat.le.at2) then
       ah=hardness(ah2,aalp2,abrat)
      else
       write(*,630)
630    format('SORRY,TEMPERATURE EXCEEDED FOR ABRASIVE MATERIAL:Termination')
       return
      endif

C     A SEPARATE SUBROUTINE TO CALCULATE THE RABINOWICZ WEAR RATE CALCULATION IS WRITTEN.
ITS NAME IS
C     'volume'. THE WORKING OF THE SUBROUTINE IS EXPLAINED IN DETAIL LATER ON.
'abrwearcoeff' IS THE
C     VARIABLE WHICH CORRESPONDS TO THE 3 BODY WEAR. THE TWO BODY WEAR HAS A VERY SIMPLE
FORMULA AND
C     HENCE NO SUBROUTINE IS NEEDED FOR THAT.

      abrwearcoeff=volume((th/ah),th)
      relwear = volume((th/ah),th)/volume((refh/ah),refh)
      twobodyrelwear = refh/th
      abrwearcoefftwobody=1/th
      write(3,640) t,relwear,twobodyrelwear,th,ah,abrwearcoeff,abrwearcoefftwobody
640   format(I4,'                ',E9.4,'                  ',E9.4,'            ',F7.1,'
',F7.1,'        ',E9.4,'        ',E9.4)

800   continue
      close(3)
      return
      end
```

A.1.2 Listing of 'subroutine hardness'

```
C     THIS SIMPLE FUNCTION DETERMINES THE HARDNESS OF THE MATERIAL WITH THE ASSUMED FORM
```

```
C       H(T)=H0*EXP(-ALPHA*T). THE INPUTS FOR THE SUBROUTINE ARE H0, ALPHA AND T

        real function hardness(h,alp,temp)
        real h,alp,rt
        integer temp

        rt=real(temp)
        hardness=h*exp(-alp*rt)
        return
        end
```

A.1.3 Listing of 'subroutine volume'

```
C       THIS SIMPLE FUNCTION DETERMINES THE RABINOWICZ WEAR RATE CALCULATION. ITS INPUTS
ARE
C       THE HARDNESS RATIO AND THE TOOL HARDNESS. THIS IS ELABORATED IN THE LITERATURE
BETTER.

        real function volume(ratio,hard)
        real ratio,hard

        if(ratio.lt.0.8) then
         volume = 1/(3*hard)
         return
        elseif(ratio.lt.1.25) then
         volume = (exp(-2.5*alog(ratio)))/(5.3*hard)
         return
        elseif(ratio.gt.1.25) then
         volume = (exp(-6.0*alog(ratio)))/(2.43*hard)
         return
        else
        endif
        return
        end
```

A.1.4 Listing of 'subroutine chemwear'

```
C       THIS IS THE MAIN SUBROUTINE WHICH COMPUTES THE CHEMICAL DISSOLUTION WEAR. ITS
INPUTS
C       ARE THE COATING, ELEMENTS ARRAY AND THE STOICHIOMETRIC NUMBER.

        subroutine chemwear(ctng,ele,x)
        character refcomp*8,ctng*8,comp*8,ele(6)*2,elem*2
        real refmlv,mlv,refl1,refm1,refn1,refl2,refm2,refn2
        real l1,m1,n1,l2,m2,n2
        integer reft1,reft2,t1,t2,freen
        integer x(6),refx(6)
        integer free(6),refree(6)
        integer i,t
        real sol,refsol,relsol

C       THE REFERENCE COMPOUND FOR THE RELATIVE WEAR CALCULATION IS THE FIRST ELEMENT IN
THE
C       CHEM1.DAT FILE. HENCE THIS CAN BE ALTERED SUITABLY.

c       READING THE DATA FOR THE REFERENCE COMPOUND
        open(unit=2,file='CHEM1.DAT',BLANK='ZERO',status='OLD')
         read(2,100) refcomp,refmlv
100      format(A8,F7.2)
         read(2,110) refl1,refm1,refn1,reft1
110      format(F10.1,F7.2,F7.2,I5)
         read(2,120) refl2,refm2,refn2,reft2
120      format(F10.1,F7.2,F7.2,I5)
        close(2)


C       THIS UNIT COLLECTS THE DATA FOR THE CANDIDATE COATING FROM THE FILE.
c       LOCATING DATA FOR THE INPUT COATING FROM THE DATA FILE
```

```
      open(unit=2,file='CHEM1.DAT',blank='ZERO',status='OLD')
160   read(2,170,end=198) comp,mlv
170    format(A8,F7.2)
       read(2,180) l1,m1,n1,t1
180    format(F10.1,F7.2,F7.2,I5)
       read(2,190,iostat=ios) l2,m2,n2,t2
190    format(F10.1,F7.2,F7.2,I5)
       if(comp.eq.ctng)then
        goto 200
        else
       endif
      goto 160
198   write(*,199)
199   format('SORRY DATA NOT AVAILABLE. COMPUTATION HALTED')
      return
200   close(2)

C     IF THE MOLAR VOLUME IS ZERO, THEN THE COMPUTATION IS HALTED FOR OBVIOUS REASONS.
c     TO SEE IF THE MOLAR VOLUME VALUE IS ZERO OR NOT
      if (mlv.eq.0) then
       write(*,201)
201    format('SORRY, THE MOLAR VOLUME IS ZERO. COMPUTATION HALTED')
       return
      else
      endif

C     THE NEXT SET OF THREE UNITS LOCATE THE EXCESS FREE ENERGY OF SOLUTION OF THE
ELEMENTS
C     IN THE COATING. AT PRESENT THREE ELEMENTS CAN BE PRESENT. IF ONLY TWO ELEMENTS ARE
PRESENT
C     THEN THE THIRD IS DUMMIED 'X' AND THE DATA CORRESPONDING TO IT IN THE FILE IS A
ZERO.

c     TO LOOK FOR THE EXCESS FREE ENERGY OF SOLUTION IN ALPHA IRON FOR THE ELEMENTS
      open(unit=2,file='ExFreeEn.DAT',blank='ZERO',status='OLD')
205    read(2,210) elem,freen
210    format(A2,I7)
       if(elem.eq.ele(1)) then
        free(1)=freen
        goto 215
       else
       endif
       goto 205
215   close(2)


      open(unit=2,file='ExFreeEn.DAT',blank='ZERO',status='OLD')
206    read(2,211) elem,freen
211    format(A2,I7)
       if(elem.eq.ele(2)) then
        free(2)=freen
        goto 216
       else
       endif
       goto 206
216   close(2)

      open(unit=2,file='ExFreeEn.DAT',blank='ZERO',status='OLD')
207    read(2,212) elem,freen
212    format(A2,I7)
       if(elem.eq.ele(3)) then
        free(3)=freen
        goto 217
       else
       endif
       goto 207
217   close(2)


C     SINCE TiN IS THE REFERENCE COATING HERE, THE APPROPRIATE CONSTANTS ARE FIXED
```

```
C       AND THE DATA COLLECTED. ONCE HAS TO REMEMBER TO CHANGE THIS IF ANOTHER COATING IS
TO BE
C       CHOSEN AS THE REFERENCE COATING. THIS WAS DELIBERATELY DONE TO KEEP THE CODE
SIMPLE.

c       FIXING THE CONSTANTS FOR THE REFERENCE MATERIAL
        refx(1)=1
        refx(2)=1
        refx(3)=0
        open(unit=2,file='ExFreeEn.DAT',blank='ZERO',status='OLD')
         read(2,218) elem,refree(1)
218      format(A2,I7)
         read(2,219) elem,refree(2)
219      format(A2,I7)
         read(2,220) elem,refree(3)
220      format(A2,I7)
        close(2)

C       THIS UNIT CREATES AN OUTPUT OF THE SOLUBILITIES. TEMPERATURE IS REPRESENTED IN
KELVIN HERE.
C       THE SUBROUTINE 'solubility' IS EXPLAINED SEPARATELY IN THE END. THE OUTPUT FILE IS
CHEMDISS.OUT
C       WHICH HAS THE APPROPRIATE HEADINGS.

c       NOW FOR CREATING THE OUTPUT OF THE SOLUBILITIES
        open(unit=2,file='chemdiss.out',blank='ZERO',status='NEW')
        write(2,400)
400     format('temp(K)    solubility  ref solubility relative solubility')
        do 490 i=1,14
        t=i*100 + 273

C       NOTE THAT TEMPERATURE HAS TO BE REPRESENTED IN KELVIN FOR CALCULATIUNG
C       THERMODYNAMIC DATA.
C       THIS UNIT COMPUTES THE SOLUBILIY OF THE CANDIDATE COATING MATERIAL. IT INVOKES
C       THE solubility FUNCTION FOR THIS. THE FUNCTION IS ELABORATED LATER ON.

        if(t.lt.t1) then
         sol=mlv*solubility(l1,m1,n1,t,x(1),x(2),x(3),free(1),free(2),free(3))
        elseif(t.lt.t2) then
         sol=mlv*solubility(l2,m2,n2,t,x(1),x(2),x(3),free(1),free(2),free(3))
        else
         write(*,410)
410      format(' SORRY TEMPERATURE EXCEEDED FOR THE COATING MATERIAL')
         return
        endif

C       THIS UNIT CALCULATES THE SOLUBILITY OF THE REFERENCE TOOL MATERIAL. DATA HAS
C       ALREADY BEEN COLLECTED FOR THIS.

        if(t.lt.reft1) then

refsol=refmlv*solubility(refl1,refm1,refn1,t,refx(1),refx(2),refx(3),refree(1),refree(2),
refree(3))
        elseif(t.lt.reft2) then

refsol=refmlv*solubility(refl2,refm2,refn2,t,refx(1),refx(2),refx(3),refree(1),refree(2),
refree(3))
        else
         write(*,420)
420      format(' SORRY TEMPERATURE EXCEEDED FOR THE REFERENCE MATERIAL')
         return
        endif
        relsol= (sol)/(refsol)
        write(2,430) t,sol,refsol,relsol
430     format(I5,'     ',E10.5,'   ',E10.5,'     ',E10.5)
490     continue
        close(2)
        return
        end
```

A.1.5 Listing of 'subroutine solubility'

```
C       THIS IS THE SUBROUTINE WHICH COMPUTES THE SOLUTBILITY IN ALPHA IRON BASED ON THE
FORMULA DEVELOPED
C       BY KRAMER AND SUH [1980] IN THEIR PAPER. IT TAKES THE THERMODYNAMIC DATA OF THE
COATING MATERIAL
C       AND RETURNS THE SOLUBILITY WHICH IS JUST A NUMBER. IT HAS TO BE CALIBRATED BASED
ON EXPERIMENTS
C       IT CAN BE SEEN THAT IT DEPENDS SENSISTIVELY WITH TEMPERATURE. FREE ENERGY OF
C       FORMATION OF THE COATING COMPOUND IS EXPRESSED IN THE FORM G=A +B LOG(T) + C.
C       AGAIN TO TAKE INTO ACCOUNT, THE PHASE CHANGE IN THE MATERIAL, TEMPERATURE IS
C       DIVIDED INTO TWO REGIMES. THE MOLAR VOLUME OF THE MATERIAL IS ALSO TO BE KNOWN
C       TO ESTIMATE THE SOLUBILITY IN VOL%. THIS ENTRY IS NEXT TO THE COMPOUND NAME IN
C       THE FILE CHEM1.DAT.

        real function solubility(sl,sm,sn,st,sx1,sx2,sx3,sfree1,sfree2,sfree3)
        real sl,sm,sn
        integer st,sx1,sx2,sx3,sfree1,sfree2,sfree3
        real rx1,rx2,rx3,rfree1,rfree2,rfree3,lnt,denom,numer,g,rt
         R=1.987

         If (sx1.lt.10) then
         rx1   =real(sx1)
         rx2   =real(sx2)
         rx3   =real(sx3)
         else
         rx1   =1.0
         rx2   =real(sx2)/ real(sx1)
         rx3   =real(sx3)/ real(sx1)
         endif

         rfree1=real(sfree1)
         rfree2=real(sfree2)
         rfree3=real(sfree3)
         rt    =real(st)
         g      =sl + (sm*rt*alog10(rt)) + (sn*rt)
         if(rx3.eq.0)then
         lnt    =rx1*alog(rx1) + rx2*alog(rx2)
         else
         lnt    =rx1*alog(rx1) + rx2*alog(rx2)+ rx3*alog(rx3)
         endif
         denom  =R*rt*(rx1 + rx2 + rx3)
         numer  =g - (rx1*rfree1) - (rx2*rfree2) - (rx3*rfree3)- R*rt*lnt
         solubility=exp(numer/denom)
        return
        end
```

A.2 Final Remarks

```
C       FINAL REMARKS: -
C       ADDING A NEW COMPOUND TO THE EXISTING LIST IS TO BE DONE AS FOLLOWS. THE
C       COMPOUND NAME WITH ITS RESPECTIVE ELEMENTS IS TO BE ADDED TO THE LIST COMP1.DAT
C       THEN THE HARDNESS OF THE COATING IS TO BE ADDED AS INDICATED IN THE MECHWEAR
C       SUBROUTINE. IF THERE ARE NEW ELEMENTS IN THE COMPOUND, THEY HAVE TO BE ENTERED
C       IN THE FILE ExFreen.DAT. THEN THE FREE ENERGY OF FORMATION OF THE COMPOUND IS
C       TO BE ENTERED IN THE FILE CHEM1.DAT AS INDICATED IN THE SUBROUTINE CHEMWEAR.
C       IF NON-STOICHIOMETRIC COMPOUNDS ARE TO BE ENTERED, IT IS SUGGESTED THAT
C       THE FRACTIONS BE NORMALIZED UPTO TWO DECIMALS AND THEN ADDED TO THE LIST AS
C       EXPLAINED BEFORE.
```

A.3 Listing of 'COMP1.DAT'

Since TiN is the reference coating in the relative wear calculation, it is the first record in the file. If some other coating is to be chosen, suitable changes are to be made

in this and other files and also in the program. In particular, the values in the variable refx(1..3) has to be changed.

```
TiN X  1 1 0TiN
TiC X  1 1 0TiC
AlO X  2 3 0Al2O3
TiC N 10 5 5TiCN
TiAlN  1 1 1TiAlN
HfC X  1 1 0HfC
ZrC X  1 1 0ZrC
TaC X  1 1 0TaC
V C X  1 1 0VC
NbC X  1 1 0NbC
SiC X  1 1 0SiC
CrC X  7 6 0Cr7C6
CrC X  3 2 0Cr3C2
MoC X  2 1 0Mo2C
AlC X  4 3 0Al4C3
B C X  4 1 0B4C
W C X  1 1 0WC
W C X  2 1 0W2C
TiO X  1 1 0TiO
TiO X  1 2 0TiO2
TiO X  2 3 0Ti2O3
TiO X  3 5 0Ti3O5
HfO X  1 2 0HfO2
ZrO X  1 2 0ZrO2
TaO X  2 5 0Ta2O5
V O X  1 1 0VO
V O X  1 2 0VO2
V O X  2 3 0V2O3
V O X  2 5 0V2O5
CrO X  1 2 0CrO2
CrO X  1 3 0CrO3
CrO X  2 3 0Cr2O3
SiO X  1 2 0SiO2
NbO X  1 1 0NbO
NbO X  1 2 0NbO2
NbO X  2 5 0Nb2O5
TiB X  1 2 0TiB2
HfB X  1 2 0HfB2
ZrB X  1 2 0ZrB2
W B X  2 5 0W2B5
A N X  1 1 0AlN
CrN X  2 1 0Cr2N
CrN X  1 1 0CrN
B N X  1 1 0BN
TaN X  1 1 0TaN
HfN X  1 1 0HfN
ZrN X  1 1 0ZrN
NbN X  2 1 0Nb2N
SiN X  3 4 0Si3N4
MoN X  2 1 0Mo2N
```

A.4 MECH1.DAT

The following is the listing of the data file containing the hardness data. As mentioned before, the hardness of the material is expressed in the form H(T) (Kg/mm^2) = $H_0e^{-\alpha T}$ where T is in °C. H_0 (in Kg/mm^2) and α are constants known from [13]. Since this may not be form of the empirical data for the whole range of temperatures from 0-1300°C, this temperature range may be divided into two ranges and separate constants may be evaluated separately for these ranges. The division in temperature ranges is taken from the third field in the records. If no division in the temperature range is needed, then the two temperatures are consecutive °C, as for example in the case of TiN. The first field stores the H_0 value and the second stores the α value while the third field stores the temperature of validity of the approximation. If the temperature in the third field of the second record is exceeded, then the computation is halted.

```
TiN
02563.6     0.001600 1200
02563.6     0.001600 1201
Fe3C
01200.0     0.001347 0400
03320.0     0.003891 1400
TiAlN
02198.4     0.000400 0600
04128.6     0.001400 1200
TiC
03300.0     0.001010 0600
10190.0     0.002890 1600
Al2O3
02468.5     0.001616 0500
03271.5     0.002180 1200
NbC
02400.0     0.001530 1600
02400.0     0.001530 1600
HfC
03000.0     0.001420 1600
03000.0     0.001420 1601
ZrC
03000.0     0.001660 1600
03000.0     0.001660 1601
TaC
01900.0     0.000775 0540
03620.0     0.001778 1600
WC
01723.9     0.001400 0400
02733.9     0.002300 1200
Mo2C
01600.0     0.001400 0350
01600.0     0.001400 0351
TiB2
```

```
03500.0     0.001890 1000
01072.0     0.000705 1600
HfB2
03000.0     0.001790 1000
01000.0     0.000686 1600
ZrB2
02300.0     0.001780 1000
00640.0     0.000495 1600
W2B5
03100.0     0.001550 1200
30720.0     0.003470 1600
TiO2
02000.0     0.000116 0600
04000.0     0.000236 0800
TiO
01250.0     0.000599 0800
01250.0     0.000599 0801
HfN
02000.0     0.000857 1000
02000.0     0.000857 1001
SiC
02800.0     0.000090 0400
04050.0     0.001010 0800
Si3N4
01950.0     0.000437 0800
01950.0     0.000437 0801
TiCN
02787.3     0.000400 0400
05496.0     0.002000 1200
```

A.5 CHEM1.DAT

This file stores the free energy of formation data. As mentioned in the remarks of the program, the Gibb's free energy of formation G (in cal/mol) of a compound is expressed in the form of equation A.1[13]: -

$$G = A + BLog_{10}(T^{\circ}K) + C \qquad \textbf{Equation A.1}$$

In addition to this value, the molar volume of the compound is also needed. This is stored next to the compound name in cm^3/mol. The values of A, B and C are stored in that order as the first three fields in each record. To take phase change into account, it may be required to split the temperature range of 373K to 1673K into two regions. The temperature of phase change is stored as the third field in the first record. The temperature beyond which this formula is not valid is stored as the third field in the second record. The computation is halted after this temperature.

```
TiN      11.49
-080250.0   00.00  22.20 1155
-080850.0   00.00  22.77 1900
TiC      12.20
-043750.0   00.00   2.41 1155
-044600.0   00.00   3.61 2000
HfC      15.04
-052165.0   00.00   1.89 2000
-052165.0   00.00   1.89 2001
ZrC      15.66
-047560.0   00.00   3.20 1135
-047995.0   00.00   3.30 2000
TaC      13.31
-035655.0   -1.48   5.41 2000
-035655.0   -1.48   5.41 2001
VC       00.91
-020540.0   00.00   1.81 2000
-050540.0   00.00   1.81 2001
NbC      13.47
-033910.0   -2.35   8.45 0950
-032940.0   00.00   0.43 2000
SiC      12.47
-014000.0   -1.30   5.68 1686
-027100.0   -2.73   18.1 2000
Cr23C6    0.0
-098280.0   00.00  -9.24 1600
-098280.0   00.00  -9.24 1601
Cr7C6     0.0
-041710.0   00.00  -6.16 1600
-041710.0   00.00  -6.16 1601
Cr3C2    27.95
-025240.0   -1.94   2.41 1600
-025240.0   -1.94   2.41 1601
Mo2C     23.78
-011330.0   -2.53   6.66 1463
-010110.0    0.00  -2.15 1600
Al4C3     0.0
-051600.0   00.00  10.00 0932
-003700.0   00.00  23.00 2000
B4C      21.75
-011413.0   04.65 -13.65 2000
-014313.0   04.65 -13.65 2001
WC       12.40
-009000.0   00.00   0.40 2000
-009000.0   00.00   0.40 2001
W2C       0.0
-014335.0  -54.26 141.11 2000
-014335.0  -54.26 141.11 2001
TiO      12.96
-123800.0   00.00  22.30 1950
-123800.0   00.00  22.30 1951
TiO2     18.76
-225000.0   00.00  45.00 1950
-225000.0   00.00  45.00 1951
Ti2O3    31.26
-363000.0   00.00  65.00 1950
-363000.0   00.00  65.00 1951
```

```
Ti3O5     0.0
-592500.0   00.00 108.33 1950
-592500.0   00.00 108.33 1951
HfO2     20.45
-266000.0   00.00  45.71 2500
-266000.0   00.00  45.71 2501
ZrO2     22.0
-262000.0   00.00  45.00 0135
-262000.0   00.00  45.00 2136
Ta2O5     0.0
-490000.0   00.00 104.88 2200
-490000.0   00.00 104.88 2201
VO        0.0
-099000.0   00.00  18.57 2200
-099000.0   00.00  18.57 2201
VO2       0.0
-168000.0   00.00  37.42 1800
-168000.0   00.00  37.42 1801
V2O3      0.0
-294000.0   00.00  59.22 2200
-294000.0   00.00  59.22 2201
V2O5      0.0
-374210.0   00.00 105.26 0950
-140670.0   00.00  59.22 2201
CrO2      0.0
-142000.0   00.00  44.0  1650
-142000.0   00.00   4.0  1651
CrO3      0.0
-138000.0   00.00  60.0  0450
-123000.0   00.00  30.0  1000
Cr2O3     0.0
-267450.0   00.00  60.97 2150
-267450.0   00.00  60.97 2151
SiO2      0.0
-215600.0   00.00  41.5  1700
-227700.0   00.00  48.7  2000
Al2O3    25.72
-400810.0   -3.98  87.64 0923
-405760.0   -3.75  92.22 1800
NbO       0.0
-096000.0   00.00  18.93 3050
-096000.0   00.00  18.93 3051
NbO2      0.0
-188000.0   00.00  35.71 3200
-188000.0   00.00  35.71 3201
Nb2O5     0.0
-452500.0   00.00  97.62 1750
-452500.0   00.00  97.62 1751
TiB2     15.42
-067230.0   00.00   4.08 1155
-068580.0   00.00   5.25 2000
HfB2     19.06
-078405.0   00.00   2.43 2000
-078405.0   00.00   2.43 2001
ZrB2     18.50
-077400.0    3.12  -6.09 1135
-076560.0    6.94 -18.35 2000
```

```
AlN      12.58
-072170.0   00.00  23.30 0932
-073750.0   00.00  25.00 2000
Cr2N      0.0
-022000.0   00.00  12.00 2000
-022000.0   00.00  12.00 2001
CrN       0.0
-027000.0   -2.08  24.44 1800
-027000.0   -2.08  24.44 1801
BN        7.13
-063000.0   -4.40  37.55 2000
-063000.0   -4.40  37.55 2001
TaN      13.74
-058380.0   -1.76  25.51 2000
-058380.0   -1.76  25.51 2001
HfN      13.95
-088716.0   -2.44  30.39 1600
-088716.0   -2.44  30.39 1800
ZrN      14.42
-087000.0   00.00  22.31 1135
-087925.0   00.00  23.11 2000
Nb2N      0.0
-056750.0   00.00  22.50 0600
-056750.0   00.00  22.50 0601
Si3N4    44.11
-177000.0   -5.76  96.30 1686
-209000.0   00.00  96.80 1973
Mo2N      0.0
-017200.0   -4.60  28.95 1300
-017200.0   -4.60  28.95 1301
VN       10.82
-041360.0   -1.32  15.65 2000
-041360.0   -1.32  15.65 2001
TiCN     11.85
-062000.0   00.00  10.93 1155
-062725.0   00.00  11.81 1900
```

A.6 ExFreeEn.DAT

This stores the excess free energy of solution of the tool constituent atoms in α-iron. It is therefore valid only for iron based work materials. Since 'X' is a dummy element, the corresponding value is zero.

```
Ti  -6900
N    5700
X       0
C    7600
Hf  -2100
Si -16700
Zr  -5000
V   -9100
Nb   -100
Ta   -200
Cr   2200
```

```
Mo  -5000
W   -7110
Al -10700
B   -2100
O  -12600
```

A.7 Results of the computer program

Since in the experimental work carried out TiN, TiCN and Al_2O_3 coatings were used, the results pertaining to only these three materials is presented here. Kramer and Kwon[13] had used the bulk hardness of the materials in their wear prediction. However, the presence of residual stresses in the thin film coating can markedly change these values [31]. Hence the arduous task of procuring the hardness data of the coatings was undertaken. While the hardness data for the TiN and the TiCN coatings was obtained from Santhanam [32], the hardness data for the Al_2O_3 coating was obtained from Quinto and Mehrotra [41]. Hardness of cementite used by Kramer and Kwon [13] was obtained from Gove and Charles [43]. The hardness data were then curve fitted and used for the theoretical wear prediction. The following sections will detail the output generated for the various coatings. The thermodynamic data for TiN and Al_2O_3 was taken from Kramer and Kwon[13]. The calculation of the thermodynamic data for the TiCN coating is detailed in Appendix B.

Table A.1: mechwear.out for the TiN coating

Temperature (°C)	Relative Abrasive wear	Two body relative wear	T/Hardness	A/Hardness	wear coeff. (3-body)	Wear coeff. (2-body).
0	1.00E+00	1.00E+00	2563.6	1200	1.69E-06	3.90E-04
100	1.00E+00	1.00E+00	2184.6	1063	2.50E-06	4.58E-04
200	1.00E+00	1.00E+00	1861.6	941.6	3.70E-06	5.37E-04
300	1.00E+00	1.00E+00	1586.3	834.1	5.48E-06	6.30E-04
400	1.00E+00	1.00E+00	1351.8	738.9	8.12E-06	7.40E-04
500	1.00E+00	1.00E+00	1151.9	576.4	5.61E-06	8.68E-04
600	1.00E+00	1.00E+00	981.6	406.1	2.10E-06	1.02E-03
700	1.00E+00	1.00E+00	836.5	286.1	7.88E-07	1.20E-03
800	1.00E+00	1.00E+00	712.8	201.6	2.95E-07	1.40E-03
900	1.00E+00	1.00E+00	607.4	142	1.11E-07	1.65E-03
1000	1.00E+00	1.00E+00	517.6	100.1	4.15E-08	1.93E-03
1100	1.00E+00	1.00E+00	441.1	70.5	1.56E-08	2.27E-03
1200	1.00E+00	1.00E+00	375.8	49.7	5.84E-09	2.66E-03

Table A-2: mechwear.out for the TiCN coating

Temperature (°C)	Relative Abrasive wear	Two body relative wear	T/Hardness	A/Hardness	wear coeff. (3-body)	Wear coeff. (2-body).
0	5.57E-01	9.20E-01	2787.3	1200	9.40E-07	3.59E-04
100	2.40E-01	8.16E-01	2678	1063	6.01E-07	3.73E-04
200	1.04E-01	7.24E-01	2573	941.6	3.84E-07	3.89E-04
300	4.48E-02	6.42E-01	2472.1	834.1	2.46E-07	4.05E-04
400	1.93E-02	5.69E-01	2375.2	738.9	1.57E-07	4.21E-04
500	1.95E-02	5.70E-01	2021.9	576.4	1.09E-07	4.95E-04
600	2.58E-02	5.93E-01	1655.4	406.1	5.42E-08	6.04E-04
700	3.41E-02	6.17E-01	1355.3	286.1	2.69E-08	7.38E-04
800	4.51E-02	6.42E-01	1109.6	201.6	1.33E-08	9.01E-04
900	5.97E-02	6.69E-01	908.5	142	6.61E-09	1.10E-03
1000	7.90E-02	6.96E-01	743.8	100.1	3.28E-09	1.34E-03
1100	1.05E-01	7.24E-01	609	70.5	1.63E-09	1.64E-03
1200	1.38E-01	7.54E-01	498.6	49.7	8.07E-10	2.01E-03

Table A-3: mechwear.out for the Al2O3 coating

Temperature (°C)	Relative Abrasive wear	Two body relative wear	T/Hardness	A/Hardness	wear coeff. (3-body)	Wear coeff. (2-body).
0	1.30E+00	1.04E+00	2468.5	1200	2.20E-06	4.05E-04
100	1.32E+00	1.04E+00	2100.2	1063	3.30E-06	4.76E-04
200	1.33E+00	1.04E+00	1786.8	941.6	4.93E-06	5.60E-04
300	1.35E+00	1.04E+00	1520.2	834.1	7.39E-06	6.58E-04
400	1.36E+00	1.05E+00	1293.3	738.9	1.11E-05	7.73E-04
500	1.38E+00	1.05E+00	1100.3	576.4	7.73E-06	9.09E-04
600	2.07E+00	1.11E+00	884.5	406.1	4.36E-06	1.13E-03
700	3.11E+00	1.18E+00	711.2	286.1	2.45E-06	1.41E-03
800	4.67E+00	1.25E+00	571.9	201.6	1.38E-06	1.75E-03
900	7.01E+00	1.32E+00	459.9	142	7.76E-07	2.17E-03
1000	1.05E+01	1.40E+00	369.8	100.1	4.37E-07	2.70E-03
1100	1.58E+01	1.48E+00	297.4	70.5	2.46E-07	3.36E-03
1200	2.37E+01	1.57E+00	239.1	49.7	1.38E-07	4.18E-03

Table A-4: chemdiss.out for the TiN coating

temp(K)	vol.solubility	vol.ref.solubility	relative solubility
373	2.12E-20	2.12E-20	1.00E+00
473	1.67E-15	1.67E-15	1.00E+00
573	2.57E-12	2.57E-12	1.00E+00
673	4.47E-10	4.47E-10	1.00E+00
773	2.04E-08	2.04E-08	1.00E+00
873	3.90E-07	3.90E-07	1.00E+00
973	4.05E-06	4.05E-06	1.00E+00
1073	2.72E-05	2.72E-05	1.00E+00
1173	1.34E-04	1.34E-04	1.00E+00
1273	5.14E-04	5.14E-04	1.00E+00
1373	1.62E-03	1.62E-03	1.00E+00
1473	4.36E-03	4.36E-03	1.00E+00
1573	1.04E-02	1.04E-02	1.00E+00
1673	2.22E-02	2.22E-02	1.00E+00

Table A-5: chemdiss.out for the TiCN coating

temp(K)	vol.solubility	vol.ref.solubility	relative solubility
373	2.12E-16	2.12E-20	1.00E+04
473	1.42E-12	1.67E-15	8.50E+02
573	4.38E-10	2.57E-12	1.71E+02
673	2.46E-08	4.47E-10	5.51E+01
773	4.88E-07	2.04E-08	2.39E+01
873	4.88E-06	3.90E-07	1.25E+01
973	3.04E-05	4.05E-06	7.51E+00
1073	1.35E-04	2.72E-05	4.95E+00
1173	4.25E-04	1.34E-04	3.17E+00
1273	1.22E-03	5.14E-04	2.37E+00
1373	3.00E-03	1.62E-03	1.85E+00
1473	6.52E-03	4.36E-03	1.50E+00
1573	1.28E-02	1.04E-02	1.24E+00
1673	2.34E-02	2.22E-02	1.05E+00

Table A-6: chemdiss.out for the Al_2O_3 coating

temp(K)	vol.solubility	vol.ref.solubility	relative solubility
373	2.25E-36	2.12E-20	1.06E-16
473	6.29E-28	1.67E-15	3.77E-13
573	1.97E-22	2.57E-12	7.65E-11
673	1.43E-18	4.47E-10	3.19E-09
773	1.03E-15	2.04E-08	5.05E-08
873	1.65E-13	3.90E-07	4.23E-07
973	9.45E-12	4.05E-06	2.33E-06
1073	2.63E-10	2.72E-05	9.64E-06
1173	4.14E-09	1.34E-04	3.08E-05
1273	4.22E-08	5.14E-04	8.21E-05
1373	3.07E-07	1.62E-03	1.90E-04
1473	1.70E-06	4.36E-03	3.90E-04
1573	7.58E-06	1.04E-02	7.33E-04
1673	2.83E-05	2.22E-02	1.27E-03

Appendix B

COMPUTATION OF THE FREE ENERGY OF FORMATION OF TiCN

B.1. Balinit B coating of Balzers

The TiCN coating was a commercial coating designated Balinit B[1]. Though it is common to represent the compound as TiCN, in reality, it exists as $TiC_{1-x}N_x$ depending on the process parameters such as the N_2 partial pressure in the PVD coating process. Hence, the free energy of formation is a separate calculation for the purpose of computing the dissolution wear.

It can be seen in [34] that a mixture of TiC and TiN in the required proportions can form TiCN. It is also known that they exhibit very good miscibility in one another and the resulting mixture shows a color according to the final stoichiometry. At a composition of $TiC_{0.5}N_{0.5}$ the compound is gray with a bluish tinge, as was the case for the coating in this work. One can therefore assume reaction in equation B.1 for the formation of $TiC_{1-x}N_x$. As a result, the free energy of formation of $TiC_{1-x}N_x$ is given by equation B.2.

$$(1-x)\langle TiC\rangle + xTiN \rightleftarrows \langle TiC_{1-x}N_x\rangle$$ **Equation B.1**

$$\Delta G_f^{\,0}\langle \mathrm{TiC_{1-x}N_x}\rangle = (1-\mathrm{x})\,\Delta G_f^{\,0}\langle \mathrm{TiCN}\rangle + x\Delta G_f^{\,0}\langle \mathrm{TiN}\rangle + RT\big(xLnx + (1-x)Ln(1-x)\big)$$

Equation B.2

Essentially, this would mean a neglect of the excess free energy of solution of the respective components in the formation of the final compound. Since, the exact composition itself was speculative, as known from Balzers, Inc., this simple assumption

[1] Coutesy Balzers, Inc.

would suffice for the computation in this context. For a more detailed study one is referred to [34], [35] and [36].

B.2. Final Form for the Free energy of formation for $TiC_{0.5}N_{0.5}$

For a value of $x = 0.5$, the formula for the free energy of formation (in Kcal/mol) appears as: -

$$\Delta G_f^0\langle TiC_{0.5}N_{0.5}\rangle = -1.37728\ T + 0.5\ (-43750 + 2.41\ T) + 0.5\ (-80250 + 22.2\ T)\ ,\ T < 1155^\circ C$$

$$\Delta G_f^0\langle TiC_{0.5}N_{0.5}\rangle = -1.37728\ T + 0.5(-44600 + 3.61\ T) + 0.5(-80850 + 22.77\ T),\ 1155^\circ K < T < 1900^\circ K$$

B.3. Molar Volume of $TiC_{1-x}N_x$

The molar volume can be obtained as a linear interpolation between the two values. This is justified because both TiN and TiC exhibit the same crystal structure and also because they have comparable molar volume values. Hence

$$MV_{TiC_{1-x}N_x} = (1-x)MV_{TiC} + xMV_{TiN} \qquad \textbf{Equation B.3}$$

A linear interpolation for $TiC_{0.5}N_{0.5}$ would therefore give rise to a molar volume of 11.85 cm^3/mol.

Appendix C

EXPERIMENTAL DATA

Insert Designation	Work Material	Coating Material	Flank Temperature (°C)	Experimental Flank Volume Wear Rate (μm^2/min)	A value	Predicted Flank Volume Wear Rate (μm^2/min)
	1018(sp)	TiN				
xnf1018sp-2			893.26	2.86	2.84E+07	3.36
xnf1018sp-3			1104.70	3.27		0.42
xnf1018sp-1			1176.60	1.09		0.21
xnf1018sp-4			1230.10	2.46		0.12
		TiCN				
xca1018sp-1			863.99	1.65	2.06E+08	1.75
xca1018sp-2			1041.40	0.40		0.51
xca1018sp-3			1103.80	0.86		0.33
xca1018sp-4			1198.20	0.69		0.17
		Al_2O_3				
xoa1018sp-2			914.87	12.14	1.64E+07	11.70
xoa1018sp-1			923.92	9.29		11.11
xoa1018sp-4			996.56	8.01		7.31
xoa1018sp-3			1054.90	7.14		5.23
	1045(sp)	TiN				
xng1045sp-1			860.53	4.80	3.01E+07	4.92
xng1045sp-2			911.54	1.93		2.98
xng1045sp-4			991.37	3.84		1.36
xng1045sp-3			1000.60	1.52		1.25
		TiCN				
xcb1045sp-2			816.93	1.44	1.63E+08	1.93
xcb1045sp-1			851.68	1.02		1.51
xcb1045sp-3			874.53	1.74		1.29
xcb1045sp-4			997.86	2.61		0.54
		Al_2O_3				
xob1045sp-1			841.48	13.81	1.24E+07	13.45
xob1045sp-4			913.39	6.26		8.90
xob1045sp-2			914.74	10.10		8.83
xob1045sp-3			933.89	8.85		7.91

Insert Designation	Work Material	Coating Material	Flank Temperature (°C)	Experimental Flank Volume Wear Rate (μm^2/min)	A value	Predicted Flank Volume Wear Rate (μm^2/min)
	1065(sp)	TiN				
xnh1065sp-2			897.61	12.69	1.23E+08	13.99
xnh1065sp-3			1002.40	7.03		5.01
xnh1065sp-1			1065.70	4.70		2.69
xnh1065sp-4			1125.30	3.27		1.50
		TiCN				
xcc1065sp-1			812.96	2.71	2.47E+08	3.01
xcc1065sp-2			911.71	1.07		1.51
xcc1065sp-4			1037.80	2.10		0.62
xcc1065sp-3			1057.10	1.81		0.54
		Al_2O_3				
xoc1065sp-1			803.55	23.04	1.77E+07	23.94
xoc1065sp-2			871.91	17.34		16.16
xoc1065sp-4	Third cut with Al_2O_3 on 1065(sp) invalid.		990.50	8.47		8.17
	1095(sp)	TiN				
xni1095sp-1			736.32	6.97		94.26
xni1095sp-2			867.06	24.89	1.71E+08	26.15
xni1095sp-3			1079.20	11.72		3.26
xni1095sp-4			1230.80	7.90		0.74
		TiCN				
xcd1095sp-1			803.92	1.40	1.63E+08	2.11
xcd1095sp-2			899.87	1.37		1.08
xcd1095sp-3			1042.60	2.40		0.40
xcd1095sp-4			1098.60	1.84		0.27
		Al_2O_3				
xod1095sp-1			736.36	29.11	1.38E+07	27.41
xod1095sp-2			801.79	13.08		18.81
xod1095sp-3			937.46	14.69		8.62
xod1095sp-4			968.57	8.44		7.21

Insert Designation	Work Material	Coating Material	Flank Temperature (°C)	Experimental Flank Volume Wear Rate (μm^2/min)	A value	Predicted Flank Volume Wear Rate (μm^2/min)
	1018(unsph)	TiN				
xnl1018un-2			857.95	5.65	1549.90	2.39
xnl1018un-1			858.39	1.41		2.39
xnl1018un-4			876.11	3.14		2.46
xnl1018un-3			994.23	0.57		2.97
		TiCN				
xcl1018un-1			782.49	1.42	663.83	0.58
xcl1018un-2			878.32	1.36		0.70
xcl1018un-3			920.70	1.03		0.76
xcl1018un-4			1165.70	0.32		1.24
		Al_2O_3				
xol1018un-1			805.01	4.10	3291.60	5.82
xol1018un-2			839.64	5.31		6.28
xol1018un-3			887.68	8.50		6.97
xol1018un-4			904.75	7.99		7.23
	1045(unsph)	TiN				
xnm1045un-2			969.39	4.66	2430.74	4.47
xnm1045un-4			1056.00	2.84		5.14
xnm1045un-3			1057.60	10.82		5.15
xnm1045un-1			1114.50	2.41		5.64
		TiCN				
xcm1045un-1			945.02	0.65	325.98	0.39
xcm1045un-2			1009.50	0.77		0.45
xcm1045un-3			1073.40	0.51		0.51
xcm1045un-4			1223.60	0.33		0.69
		Al_2O_3				
	First cut interrupted due to BUE					
xom1045un-4			978.28	6.43	2221.19	5.73
xom1045un-3			1023.60	6.69		6.32
xom1045un-2			1205.50	8.71		9.38

Insert Designation	Work Material	Coating Material	Flank Temperature (°C)	Experimental Flank Volume Wear Rate (μm^2/min)	A value	Predicted Flank Volume Wear Rate (μm^2/min)
	1070(unsph)	TiN				
xnn1070un-4			834.19	2.78	1235.24	1.83
xnn1070un-3			862.14	1.20		1.92
xnn1070un-1			962.28	1.50		2.25
xnn1070un-2			1134.40	3.41		2.96
		TiCN				
xcn1070un-2			1020.70	1.25	624.51	0.87
xcn1070un-4			1021.40	1.24		0.88
xcn1070un-1			1025.30	0.59		0.88
xcn1070un-3			1101.40	0.64		1.03
		Al_2O_3				
xon1070un-3			860.04	6.44	3521.31	7.02
xon1070un-2			919.23	11.27		7.98
xon1070un-4			937.11	6.78		8.30
xon1070un-1			937.36	7.16		8.31

Insert Designation	Work Material	Coating Material	Cutting Speed (m/min)	Crater Temperature (°C)	Experimental Crater Wear Rate (μm/min)	A and B Values	Predicted Crater Wear Rate (μm/min)
	1018(sp)	TiN					
xnf1018sp-2			164.30	1037.40	2.81	587451.93	2.79
xnf1018sp-3			239.57	1274.98	0.29	1.09	0.57
xnf1018sp-1			99.29	1355.76	1.84		0.33
xnf1018sp-4			274.09	1415.88	0.43		0.88
		TiCN					
xca1018sp-1			101.32	1004.52	0.42	1696057.67	0.56
xca1018sp-2			164.05	1203.85	0.64	1.31	0.33
xca1018sp-3			274.44	1273.97	0.59		0.49
xca1018sp-4			215.81	1380.03	0.52		0.63
		Al_2O_3					
xoa1018sp-2			164.54	1061.69	0.98	19553.11	1.01
xoa1018sp-1			102.06	1071.85	0.36	16425.43	0.60
xoa1018sp-4			207.55	1153.47	1.20		0.91
xoa1018sp-3			292.08	1219.02	1.38		1.44
	1045(sp)	TiN					
xng1045sp-1			100.08	1000.63	0.11	31276.25	0.20
xng1045sp-2			162.36	1057.94	0.35	16.13	0.30
xng1045sp-4			289.04	1147.64	0.99		0.78
xng1045sp-3			225.68	1158.01	0.53		0.75
		TiCN					
xcb1045sp-2			164.33	951.64	0.16	94713.57	0.25
xcb1045sp-1			100.87	990.69	0.16	21.56	0.25
xcb1045sp-3			227.44	1016.36	0.63		0.47
xcb1045sp-4			291.11	1154.93	1.67		1.69
		Al_2O_3					
xob1045sp-1			100.14	979.22	0.73	18200.42	0.93
xob1045sp-4			292.11	1060.02	2.20	169999.48	1.96
xob1045sp-2			164.92	1061.54	1.03		1.17
xob1045sp-3			227.88	1083.06	1.50		1.58

Insert Designation	Work Material	Coating Material	Cutting Speed (m/min)	Crater Temperature (°C)	Experimental Crater Wear Rate (μm/min)	A and B Values	Predicted Crater Wear Rate (μm/min)
	1065(sp)	TiN					
xnh1065sp-2			170.22	1042.29	1.00	288673.03	1.43
xnh1065sp-3			219.21	1160.03	2.08	8.96	0.93
xnh1065sp-1			103.18	1231.16	0.58		0.71
xnh1065sp-4			261.37	1298.12	1.88		2.05
		TiCN					
xcc1065sp-1			103.88	947.18	0.19	720387.67	0.44
xcc1065sp-2			157.73	1058.13	0.86	12.78	0.55
xcc1065sp-4			241.14	1199.81	1.82		1.46
xcc1065sp-3			218.50	1221.49	1.25		1.62
		Al_2O_3					
xoc1065sp-1			105.56	936.61	0.61	14281.05	0.95
xoc1065sp-2			157.66	1013.42	1.31	75382.09	0.95
xoc1065sp-4	Third cut with Al_2O_3 on 1065(sp) invalid.		257.82	1146.66	1.45		1.47
	1095(sp)	TiN					
xni1095sp-1			104.24	861.07	1.07	99912.14	1.69
xni1095sp-2			168.79	1007.97	2.08	6.48	0.69
xni1095sp-3			231.48	1246.33	2.73		0.83
xni1095sp-4			277.21	1416.66	4.29		4.60
		TiCN					
xcd1095sp-1			105.04	937.02	1.04	2047747.12	1.23
xcd1095sp-2			170.14	1044.83	1.73	21.99	1.31
xcd1095sp-3			231.48	1205.20	2.05		2.70
xcd1095sp-4			279.45	1268.12	4.91		4.61
		Al_2O_3					
xod1095sp-1			107.73	861.11	1.05	12931.57	1.36
xod1095sp-2			171.11	934.63	1.79	667761.79	1.47
xod1095sp-3			234.40	1087.07	2.69		2.76
xod1095sp-4			274.74	1122.02	5.14		5.11

Insert Designation	Work Material	Coating Material	Cutting Speed (m/min)	Crater Temperature (°C)	Experimental Crater Wear Rate (μm/min)	A and B Values	Predicted Crater Wear Rate (μm/min)
	1018(unsph)	TiN					
xnl1018un-2			154.40	997.73	2.73	173944.51	1.15
xnl1018un-1			90.90	998.22	0.89	1.10	0.67
xnl1018un-4			275.60	1018.13	0.50		1.68
xnl1018un-3			214.30	1150.85	0.43		0.39
		TiCN					
xcl1018un-1			91.00	912.94	0.07	769522.06	0.43
xcl1018un-2			153.00	1020.62	0.38	1.63	0.36
xcl1018un-3			214.00	1068.24	0.83		0.38
xcl1018un-4			275.70	1343.52	0.61		0.64
		Al_2O_3					
xol1018un-1			92.00	938.25	0.12	947.45	0.09
xol1018un-2			153.30	977.16	0.10	536148.45	0.19
xol1018un-3			214.80	1031.13	0.70		0.54
xol1018un-4			275.30	1050.31	0.79		0.87
	1045(unsph)	TiN					
xnm1045un-2			164.30	1122.94	0.74	575105.30	1.35
xnm1045un-4			274.50	1220.26	2.56	7.32	1.44
xnm1045un-3			221.90	1222.06	1.19		1.23
xnm1045un-1			91.60	1285.99	0.14		0.93
		TiCN					
xcm1045un-1			91.60	1095.56	0.05	940325.38	0.26
xcm1045un-2			152.60	1168.01	0.37	4.63	0.43
xcm1045un-3			220.60	1239.81	1.12		0.77
xcm1045un-4			276.70	1408.57	2.68		2.74
		Al_2O_3					
		First cut interrupted due to BUE					
xom1045un-4			284.10	1132.93	2.33	41731.31	2.42
xom1045un-3			221.00	1183.85	1.58	1202.08	1.42
xom1045un-2			152.20	1388.24	1.09		1.10

nsert Designation	Work Material	Coating Material	Cutting Speed (m/min)	Crater Temperature (°C)	Experimental Crater Wear Rate (μm/min)	A and B Values	Predicted Crater Wear Rate (μm/min)
	1070(unsph)	TiN					
xnn1070un-4			272.40	971.03	1.17	101401.29	1.55
xnn1070un-3			214.50	1002.44	1.34	5.32	0.92
xnn1070un-1			90.30	1114.96	2.00		0.21
xnn1070un-2			152.30	1308.35	0.81		0.98
		TiCN					
xcn1070un-2			152.80	1180.60	0.61	8436722.04	1.42
xcn1070un-4			271.90	1181.38	3.02	3.33	2.42
xcn1070un-1			92.00	1185.76	0.15		0.88
xcn1070un-3			214.00	1271.27	1.71		1.47
		Al_2O_3					
xon1070un-3			213.50	1000.08	2.37	24944.38	2.37
xon1070un-2			152.50	1066.58	0.65	99651.56	1.29
xon1070un-4			275.00	1086.67	2.65		2.13
xon1070un-1			92.90	1086.96	0.46		0.80

Insert Designation	Work Material	Coating Material	Cutting Speed (m/min)	Crater Area (mm^2)	Fracture Toughness (J) [37]
	1018(sp)	TiN			
xnf1018sp-1			99.29	3.45	120.0
xnf1018sp-2			164.30	4.13	
xnf1018sp-3			239.57	2.95	Average Area =
xnf1018sp-4			274.09	2.51	3.26
		TiCN			
xca1018sp-1			101.32	3.81	
xca1018sp-2			164.05	3.24	
xca1018sp-4			215.81	3.28	Average Area =
xca1018sp-3			274.44	2.85	3.30
		Al_2O_3			
xoa1018sp-1			102.06	3.60	
xoa1018sp-2			164.54	3.49	
xoa1018sp-4			207.55	3.36	Average Area =
xoa1018sp-3			292.08	2.86	3.33
	1045(sp)	TiN			
xng1045sp-1			100.08	2.99	30.6
xng1045sp-2			162.36	2.87	
xng1045sp-3			225.68	2.23	Average Area =
xng1045sp-4			289.04	2.17	2.57
		TiCN			
xcb1045sp-1			100.87	3.31	
xcb1045sp-2			164.33	3.06	
xcb1045sp-3			227.44	2.49	Average Area =
xcb1045sp-4			291.11	2.17	2.76
		Al_2O_3			
xob1045sp-1			100.14	3.45	
xob1045sp-2			164.92	2.98	
xob1045sp-3			227.88	2.76	Average Area =
xob1045sp-4			292.11	2.74	2.98

Insert Designation	Work Material	Coating Material	Cutting Speed (m/min)	Crater Area (mm^2)	Fracture Toughness (J)
	1065(sp)	TiN			
xnh1065sp-1			103.18	2.55	10.0
xnh1065sp-2			170.22	2.86	
xnh1065sp-3			219.21	2.45	Average Area =
xnh1065sp-4			261.37	2.14	2.50
		TiCN			
xcc1065sp-1			103.88	3.16	
xcc1065sp-2			157.73	2.07	
xcc1065sp-3			218.50	2.16	Average Area =
xcc1065sp-4			241.14	2.74	2.53
		Al_2O_3			
xoc1065sp-1			105.56	3.21	
xoc1065sp-2			157.66	3.12	Average Area =
xoc1065sp-4	Third cut with Al_2O_3 on 1065(sp) invalid.		257.82	2.30	2.88
	1095(sp)	TiN			
xni1095sp-1			104.24	3.47	2.7
xni1095sp-2			168.79	2.52	
xni1095sp-3			231.48	1.92	Average Area =
xni1095sp-4			277.21	2.13	2.51
		TiCN			
xcd1095sp-1			105.04	2.78	
xcd1095sp-2			170.14	2.33	
xcd1095sp-3			231.48	2.01	Average Area =
xcd1095sp-4			279.45	2.01	2.28
		Al_2O_3			
xod1095sp-1			107.73	3.56	
xod1095sp-2			171.11	2.80	
xod1095sp-3			234.40	2.47	Average Area =
xod1095sp-4			274.74	2.54	2.84

Insert Designation	Work Material	Coating Material	Cutting Speed (m/min)	Crater Area (mm^2)	Fracture Toughness (J)
	1018(unsph)	TiN			
xnl1018un-1			90.90	3.69	*******
xnl1018un-2			154.40	3.21	
xnl1018un-3			214.30	2.17	Average Area =
xnl1018un-4			275.60	2.36	2.86
		TiCN			
xcl1018un-1			91.00	3.56	
xcl1018un-2			153.00	2.75	
xcl1018un-3			214.00	2.41	Average Area =
xcl1018un-4			275.70	2.01	2.68
		Al_2O_3			
xol1018un-1			92.00	3.49	
xol1018un-2			153.30	2.97	
xol1018un-3			214.80	2.54	Average Area =
xol1018un-4			275.30	2.35	2.84
	1045(unsph)	TiN			
xnm1045un-1			91.60	2.02	**********
xnm1045un-2			164.30	2.59	
xnm1045un-3			221.90	2.03	Average Area =
xnm1045un-4			274.50	2.45	2.27
		TiCN			
xcm1045un-1			91.60	2.75	
xcm1045un-2			152.60	2.34	
xcm1045un-3			220.60	2.08	Average Area =
xcm1045un-4			276.70	1.82	2.25
		Al_2O_3			
		First cut interrupted due to BUE			
xom1045un-2			152.20	2.91	
xom1045un-3			221.00	2.49	Average Area =
xom1045un-4			284.10	2.46	2.62

Insert Designation	Work Material	Coating Material	Cutting Speed (m/min)	Crater Area (mm^2)	Fracture Toughness (J)
	1070(unsph)	TiN			
xnn1070un-1			90.30	2.99	****
xnn1070un-2			152.30	1.59	
xnn1070un-3			214.50	2.28	Average Area =
xnn1070un-4			272.40	2.26	2.28
		TiCN			
xcn1070un-1			92.00	1.90	
xcn1070un-2			152.80	1.66	
xcn1070un-3			214.00	1.53	Average Area =
xcn1070un-4			271.90	1.45	1.64
		Al_2O_3			
xon1070un-1			92.90	2.54	
xon1070un-2			152.50	2.25	
xon1070un-3			213.50	2.14	Average Area =
xon1070un-4			275.00	1.99	2.23

Appendix D

CURVE FITTED PEAK TEMPERATURE

D.1 Inverse Estimation Scheme for the Flank Temperature

IR pyrometry was adopted to measure the temperature of the tool at a fixed point on the rake face. One criticism of the method has been the effect of the chip coming in the field of view of the pyrometer [38]. Previous attempts at this approach were made by Wang et al. [42]. However, adopting the assembly shown in Figure 4.3 resolved this problem. To estimate the cutting interface temperature, Yen and Wright [26] suggested a method using a remote sensing technique. Since the coating thickness is exceedingly small to offer any thermal resistance, the same model was capable of estimating the interface temperature [39]. The flank temperature can be estimated using the scheme suggested by Oxley [29], which states that the tool work interface temperature is 0.82-0.95 times the mean chip-tool interface temperature. The average value of 0.89 times the chip-tool interface temperature was used for this study (All temperatures being in Kelvin).

Determining the steady state cutting temperature from the knowledge of the transient temperature at a point remote to the interface involves solution of the 3-D transient heat conduction problem. Since the time derivative in the heat diffusion equation is of the first order, it was inferred that the time growth in the remotely measured temperature is of the form in equation D.1.

$$T(t) = T_i + T_0(1 - e^{-\alpha t}) \qquad \textbf{Equation D.1}$$

where T_i is the initial temperature in the temperature history of the pyrometer and T_0 and α are constants derived from a curve fitting process on the temperature data of the pyrometer. Then T_i+T_0 would represent the steady state temperature of the pyrometer. The temperature measurements showed less than 2% difference between the empirical result and that obtained from the curve fitting process. In addition, the difference between the steady state temperature obtained by the above equation and the peak temperature measured by the pyrometer was less than 7°C.

The 1-D ellipsoidal mapping model simplifies the inverse problem of estimating the interfacial temperature [26]. The modeling and the governing differential equations are discussed in the referred paper. The final form of the inverse solution [40] can be expressed as in equation D.2.

$$\frac{T - T_\infty}{T_r - T_\infty} = 1 - \left(\frac{2}{\pi}\right) \tan^{-1}\left(\sqrt{\left(\frac{x}{a}\right)^2 - 1}\right) \qquad \textbf{Equation D.2}$$

where

T_r is the steady-state cutting interface temperature

T is the steady state remotely measured rake face temperature

T_∞ is the temperature in the far field of the tool (Taken to be 25°C)

x is the distance of the point of measurement from the origin of the axes

a is the radius of the circular tool-chip contact area.

BIBLIOGRAPHY

BIBLIOGRAPHY

[1] ISO Standard 3685-1977 (E), "Tool Life Testing with Single Point Turning Tools", International Organization for Standardization, 1977

[2] Ramalingham, S. and Wright, P.K., "Abrasive wear in machining: Experiments with controlled microstructure", *Journal of Materials Technology*, vol. 103, pp.151-156, ASME International, April 1981

[3] Byrd, J.D and Ferguson, B.L., "A study of the influence of hard inclusions on carbide tool wear utilizing a powder metal technique", in *Proceedings of the VIth NAMRC*, University of Florida, Gainesville, pp.310-315, 1978

[4] Brun, M.K., Lee, M., Gorsler, F., "Wear characteristics of various hard materials for machining of SiC-reinforced aluminum alloy", *Wear,* vol. 104, pp.21-29, 1985

[5] Kramer, B.M., "Predicted wear resistances of binary carbide coatings", *Journal of Vacuum Science and Technology*, vol. A4(6) Nov/Dec, pp.2870-2873, 1986

[6] Ramalingam, S. and Watson, J.D., "Tool Life Distributions *Part 4: Minor phases in work material and multiple-injury tool failure*", *Journal of Engineering for Industry*, vol. 100, pp.201-209, ASME International, 1978

[7] Kramer, B.M and Kwon, P.Y. (formerly P.K. Judd), "Computational design of wear coatings", *Journal of Vacuum Science and Technology*, vol. A3(6) Nov/Dec, pp.2439-2444, 1985

[8] Kramer, B.M. and Suh, N.P., "Tool Wear by Solution: *A quantitative understanding*", *Journal of Engineering for Industry*, vol. 102, pp.303-309, ASME International, 1980

[9] Dearnley. P.A., "Rake and Flank Wear Mechanisms of Coated and Uncoated Cemented Carbides", Journal of Engineering Materials Technology, vol. 107, pp.68-82, ASME International, 1985

[10] Cho, S.S and Komvopoulos, K., "Wear mechanisms of multi-layer coated cemented carbide cutting tools", *Journal of Tribology*, vol. 119, pp.8-17, ASME International, 1997

[11] Cook, N.H., "Tool wear and tool life", Journal of Engineering for Industry, pp.931-938, ASME International, 1973

[12] Stjernberg, K. and Thelin, A, "Wear mechanisms of coated carbide tools in the machining of steel", in *High productivity machining-Proceedings of the International Conference on high productivity machining, materials and processing*, (U.K.Sarin ed.), pp.95-104, ASM International, 1985

[13] Kramer, B.M., "On tool materials for high speed machining", *Journal of Engineering for Industry*, vol. 109, pp.87-91, ASME International, 1987

[14] Milovic, R., Smart, E.F. and Wise, M.L.H., "Comparison of the use TiN-Coated and uncoated high-speed steel and fine-grained cemented carbide tools in the cutting of resulfurized 0.08 wt-%C free-cutting steels", *Materials Science and Technology*, vol. 2, pp.59-68, 1986

[15] Chubb, J.P. and Billingham, J., "Coated cutting tools- A study of wear mechanisms in high speed machining", *Wear*, vol. 61, pp.283-293, 1980

[16] Kim, J.D., "Effect of carbide and oxide coating thickness on cutting tool wear in the turning process", *Journal of Testing and Evaluation*, vol. 23 No.4, pp.311-314, 1995

[17] Kim Sukyoung and Durham, Delcie.R., "Microscopic studies of flank wear on alumina tools", Journal of Engineering for Industry, vol. 113, pp.204-209, ASME International, 1991

[18] Lee, M and Richman, M.H., "Some properties of TiC-coated cemented tungsten carbide", *Metals Technology*, pp.538-546, 1974

[19] Suh, N.P., "Coated Carbides - Past, Present and Future, in *1976 International conference on hard material tool technology*, Pittsburgh, Pennsylvania, The Carbide Journal, Jan-Feb 1977, pp.3-9

[20] Subramaniam, S.V., Ingle, S.S. and Kay, D.A.R., "Design of coatings to minimize tool crater wear", *Surface and Coatings Technology*, vol. 61, pp.293-299, 1993

[21] Trent, E.M., "Cutting steel and iron with cemented carbide cutting tools-Parts I", *Journal of the Iron and Steel Institute*, October 1963

[22] Trent, E.M., "Cutting steel and iron with cemented carbide cutting tools-Parts II", *Journal of the Iron and Steel Institute*, November1963

[23] Trent, E.M., "Cutting steel and iron with cemented carbide cutting tools-Parts III", *Journal of the Iron and Steel Institute*, December 1963

[24] Rabinowicz, E., Dunn, L.A. and Russel, P.G., "A study of abrasive wear under three-body conditions", *Wear*, vol. 4, pp.345-355, 1961

[25] Shaw, M.C., *Metal Cutting Principles*, Oxford: Clarendon Press, 1984

[26] Yen, D.W. and Wright, P.K., "A remote temperature sensing technique for estimating the cutting interface temperature distribution", *Journal of Engineering for Industry*, vol. 108, pp.252-263, ASME International, 1986

[27] Lin, Jehnming, Chen, Tei-chen and Weng, Cheng-I, "Development of infrared pyrometer with fiber optic for measuring cutting temperature at high speed machining", in *Symposium on monitoring and control of manufacturing processes*, vol. 44, pp.17-32, ASME Winter Annual meeting, Dallas, PED, ASME International, 1990

[28] Rall, D.L. and Giedt, W.H., "Heat transfer to, and temperature distribution in a metal cutting tool", *Transactions of the ASME*, vol. 78, pp.1507-1515, ASME International, 1959

[29] Oxley, P.L.B., *The Mechanics of Machining: An Analytical approach to assessing machinability,* New York:John Wiley and Sons, 1989

[30] Boothroyd, G., Eagle, J.M. and Chisholm, A.W.J., "Effect of tool flank wear on the temperatures generated during metal cutting", in *Proceedings of the 8th International Machine tool design and research conference,* Oxford, pp.667-680, Pergamon, 1967

[31] Santhanam, A.T.; Quinto, D.T., "Surface engineering of carbide, cermet and ceramic cutting tools", in *ASM Handbook Vol. 5 Surface Engineering*, pp.900-908 ASM International, 1992

[32] Santhanam, A.T., *Private Communication,* 1997

[33] Rabinowicz, E., "Abrasive wear resistance as a materials test", Paper presented at the *JSLE, ASLE International Lubrication Conference* in Tokyo, Japan, pp.378-381, June 9-11, 1975

[34] Kieffer, R.; Ettmayer, P.; Freudhofmeier, M., 1971, *About Nitrides and Carbonitrides and Nitride-based cemented hard alloys*, in Modern developments in Powder metallurgy, H.H.Hausner (Ed.), Plenum Press, New York, pp.201-214

[35] Pastor, H., 1988, *Titanium-Carbonitride-based hard alloys for cutting tools*, Materials Science and Engineering, **A105/106**, pp.401-409

[36] Portnoi ,K.I and Levinskii, Yu.V., 1963, *High-Temperature equilibrium of the reaction between Titanium Nitride and Carbon,* Russian Journal of Physical Chemistry, **37(No.12)**, pp. 1424-1428

[37] *Metals Reference Handbook,* American Society of Metals, 2nd Edition, p.211, 1983

[38] Trent, E.M., *Metal Cutting,* Butterswoth, 1984

[39] Beck, J.V., 1997, *Private Communication*

[40] Lin, Jehnming, Lee, Shinn-Liang and Weng, Cheng-I, "Estimation of cutting temperature in high speed machining", *Journal of Engineering Materials Technology*, vol. 114, pp.289-296, 1992

[41] Mehrotra, P.K and Quinto, D.T., "Techniques for evaluating mechanical properties of hard coatings", *Journal of Vacuum Science and Technology*, vol. A3(6), pp.2401-2405, 1985

[42] Wang, L., Saito, K. and Jawahir, I.S., "Infrared Temperature Measurement of Curled Chip Formation in Metal Machining", in *Transactions of the NAMRI/SME XXIV*, pp.87-92, 1996

[43] Gove, K.B. and Charles, J.A., "The high-temperature hardness of various phases of steels", Metals Technology, pp.279-283, 1974